



HAL
open science

Encapsulation of cannabidiol in oil-in-water nanoemulsions and nanoemulsion-filled hydrogels: A structure and biological assessment study

Sotiria Demisli, Eleni Galani, Maria Goulielmaki, Fotios Kyrilis, Tanja Ilić, Farzad Hamdi, Milkica Crevar, Panagiotis Kastritis, Vasiliki Pletsas, Frédéric Nallet, et al.

► To cite this version:

Sotiria Demisli, Eleni Galani, Maria Goulielmaki, Fotios Kyrilis, Tanja Ilić, et al.. Encapsulation of cannabidiol in oil-in-water nanoemulsions and nanoemulsion-filled hydrogels: A structure and biological assessment study. *Journal of Colloid and Interface Science*, 2023, 634, pp.300-313. 10.1016/j.jcis.2022.12.036 . hal-03925004

HAL Id: hal-03925004

<https://hal.science/hal-03925004>

Submitted on 5 Jan 2023

HAL is a multi-disciplinary open access archive for the deposit and dissemination of scientific research documents, whether they are published or not. The documents may come from teaching and research institutions in France or abroad, or from public or private research centers.

L'archive ouverte pluridisciplinaire **HAL**, est destinée au dépôt et à la diffusion de documents scientifiques de niveau recherche, publiés ou non, émanant des établissements d'enseignement et de recherche français ou étrangers, des laboratoires publics ou privés.

1 **Encapsulation of cannabidiol in oil-in-water nanoemulsions and**
2 **nanoemulsion-filled hydrogels: a structure and biological assessment**
3
4 **study**
5

6 Sotiria Demisli ^{1,2}, Eleni Galani^{1,3}, Maria Goulielmaki¹, Fotios Kyrilis⁴, Tanja Ilic⁵, Farzad
7 Hamdi⁴, Milkica Crevar⁵, Panagiotis L. Kastritis⁴, Vasiliki Pletsas¹, Frédéric Nallet⁶, Snežana
8 Savić⁵, Aristotelis Xenakis¹, Vassiliki Papadimitriou^{1,*}

9 ¹*Institute of Chemical Biology, National Hellenic Research Foundation, Athens, Greece*

10 ²*Department of Biochemistry & Biotechnology, University of Thessaly, Larissa, Greece*

11 ³*Department of Food Science & Human Nutrition, Agricultural University of Athens, Greece*

12 ⁴*Martin Luther University Halle-Wittenberg, Halle (Saale), Germany*

13 ⁵*Department of Pharmaceutical Technology and Cosmetology, University of Belgrade,*
14 *Belgrade, Serbia*

15 ⁶*Centre de Recherche Paul Pascal (CRPP) UMR 5031 CNRS, University of Bordeaux, France*

31 **Abstract**

32 *Hypothesis*

33 The oral administration of lipophilic bioactives using conventional nanoemulsions presents
34 certain limitations. Hence, novel hybrid vehicles could be valuable alternatives providing
35 diverse routes of administration. To determine the suitability of a nanocarrier the elucidation
36 of its structure is essential since it affects the release of the encapsulated compound.
37 Specifically, concerning the transdermal delivery the evaluation of the penetration of the
38 bioactive through the skin is also crucial.

39 *Experiments*

40 Oil-in-water nanoemulsions (NE) and the respective nanoemulsion-filled hydrogels (NE/HG)
41 were formulated and structurally characterized as carriers of cannabidiol (CBD). The NE
42 stability and size were studied and the structure of both systems was visualized with
43 microscopic techniques to determine possible structural changes in the NE upon their
44 incorporation into the hydrogels. Potential use of the formulated nanocarriers for topical
45 application was evaluated through cytotoxicity tests over normal human skin fibroblasts. An
46 *ex vivo* permeation protocol using porcine ear skin was also implemented to assess the release
47 of CBD and its penetration through the skin.

48 *Findings*

49 Experimental results obtained by SAXS, EPR and confocal microscopy show that incorporation
50 of the NE in the hydrogels does not significantly affect their structural properties. CryoEM
51 indicated that CBD does not have observable effects on structural rigidity and ultrastructure
52 of the NE, suggesting minimal perturbations upon drug encapsulation. The proposed systems
53 did not exhibit any cytotoxicity and CBD was released effectively penetrating through the skin
54 indicating their suitability for transdermal delivery.

55
56
57 **Keywords:** nanoemulsions; hydrogels; cannabinoids; DLS; EPR; cryo-EM; SAXS; confocal
58 microscopy; cell viability; skin permeation

59

60

61

1. Introduction

Nowadays, the consumer interest is shifted towards more natural formulations for the treatment of various conditions. Particularly cannabidiol (CBD) has attracted considerable attention in recent years due to its multiple pharmacological actions. Cannabidiol is a 21-carbon terpenophenolic, non-psychoactive compound and constitutes one of the major phytocannabinoids of the *Cannabis sativa* plant extract (Figure 1) [1]. Over the years, numerous research studies have demonstrated that CBD presents good safety profile, affects various physical functions and could demonstrate promising therapeutic action to medical and conditions such as seizures, epilepsy [2], psychiatric [3] and skin conditions [4], pain and inflammation [5]. In addition, due to the anti-inflammatory [6], immunomodulatory and neuroprotective [7] properties that CBD demonstrates it was proposed as a support drug during the COVID-19 pandemic [8,9]. However, due to the wide variability of the plant composition and subsequently of the CBD extracts and the broadly diversified THC/CBD ratios their use as therapeutic agents is troublesome [10,11]. Moreover, CBD is a sensitive bioactive compound that can easily undergo degradation when in solution or in contact with light and temperature [12]. For that reason, synthetically produced CBD was selected for encapsulation in the present study.

Until now oral route has been the most preferred mode of delivery for CBD. However, this method of administration presents significant limitations due to the highly lipophilic nature of this substance including gastric instability and low oral bioavailability due to rapid elimination through first-pass metabolism [13]. Another important obstacle with oral administration is that it is not feasible for people who suffer from nausea, gastrointestinal problems or seizures. To address the aforementioned limitations research groups are focused on finding more effective methods for the administration of bioactive compounds. There are indications that one of the most advantageous approaches is the transdermal delivery since it provides the possibility of self-administration, prolonged contact with the site of action offering controlled drug delivery over extended periods of time and prevention of gastrointestinal side-effects [14]. Specifically, concerning cannabinoids the transdermal administration leading to systemic delivery could provide sustained and possibly targeted delivery [15]. In fact, the beneficial effects of transdermal delivery of CBD against diverse conditions including arthritis, seizures, and anxiety and in general the overall improvement of the quality of life of the patients have been demonstrated by various *in vivo* studies [16–18].

However, the selection of the suitable delivery route is often not enough so encapsulation in various nanocarriers is frequently preferred in order to enhance the efficacy of a bioactive

1
2
3
4
5
6
7
8
9
10
11
12
13
14
15
16
17
18
19
20
21
22
23
24
25
26
27
28
29
30
31
32
33
34
35
36
37
38
39
40
41
42
43
44
45
46
47
48
49
50
51
52
53
54
55
56
57
58
59
60
61
62
63
64
65

96 compound of interest. Commonly used nanocarriers include micelles, polymers,
97 nanoparticles, liposomes, niosomes, nanogels, and dendrimers. The main advantages of using
98 nanocarriers include improved solubility of highly hydrophobic compounds, protection
99 against degradation of sensitive bioactive molecules, and efficient delivery to their exact
100 targets [19–22]. Among different nanocarriers for the effective delivery of bioactive
101 compounds, nanoemulsions based on biocompatible materials have been extensively studied
102 by many research teams worldwide mainly due to their physicochemical properties [23,24].
103 Nanoemulsions (NE) are fine oil-in-water (O/W) or water-in-oil (W/O) dispersions stabilized
104 by an interfacial film of surfactant molecules forming droplets of nanometric sizes. The oily
105 phase usually consists of different types of lipids and oils. The aqueous phase consists of water
106 or can be formulated by adding different water-soluble components. Surfactants are the
107 molecules that adsorb into oil/water interfaces reducing the interfacial tension and stabilizing
108 the emulsions. Nanoemulsions are thermodynamically unstable systems and can be prepared
109 by both low and high-energy methods. Low energy methods include self-emulsification and
110 phase inversion whereas high energy methods include high-pressure homogenization,
111 microfluidization and ultrasonication [25,26]. The main advantages of nanoemulsions for the
112 effective delivery and release of bioactive components are their low surfactant-to-oil ratio,
113 the increased water-solubility, stability, and bioavailability of the encapsulated lipophilic
114 molecules, as well as their administration through various routes [19,25].

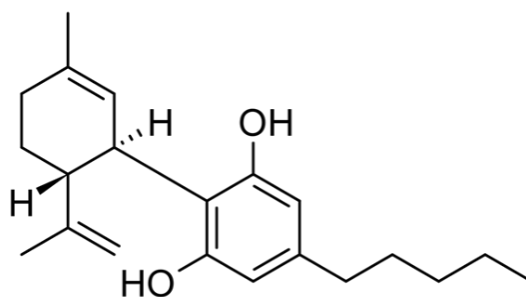
115 Hydrogels (HG) are composed of natural or synthetic hydrophilic polymers that are cross-
116 linked forming three-dimensional networks with the ability to retain large amounts of water.
117 Due to their properties such as high water content, flexibility and biocompatibility they are
118 popular for many biomedical applications including drug delivery [27,28]. Chitosan hydrogels
119 is a class of hydrogels based on chitosan, a cationic natural polymer obtained by deacetylation
120 of chitin. These hydrogels are of special interest due to their appealing physicochemical,
121 biological, and mechanical properties [29]. Chitosan hydrogels are biocompatible,
122 biodegradable, with low toxicity and low cost. Moreover, they are easy to handle and present
123 mucoadhesive properties providing prolonged contact with the site of action. In addition,
124 chitosan hydrogels are promising absorption enhancers of active compounds through
125 constructed epithelia [30]. Despite their advantages, hydrogels are not often used as delivery
126 vehicles of bioactive molecules due to their inability to encapsulate lipophilic substances and
127 their possible toxicity as a result of burst release [31]. Nanoemulsions on the other hand
128 present some limitations such as low viscosity and low spreadability making them less

129 appropriate for (trans)dermal or other applications requiring adherence and prolonged
130 contact with the site of action.

131 Hence, due to the limitations of the two aforementioned nanocarriers, recently there is a
132 growing interest towards their combination resulting in a novel hybrid system the
133 nanoemulsion-filled hydrogels or emulgels (NE/HG). Specifically, nanoemulsion-filled
134 hydrogels consist of a polymer gel matrix in which a nanoemulsion is incorporated [32]. These
135 systems possess different properties compared to the initial nanocarriers such as improved
136 stability, and versatile texture [33]. In addition, they present various advantages over
137 nanoemulsions and hydrogels since they can encapsulate both lipophilic and hydrophilic
138 bioactive compounds, provide controlled release, increase biocompatibility and improve the
139 release profile of the incorporated nanoemulsion [31,34,35].

140 The aim of the present study was to develop stable, biocompatible oil-in-water
141 nanoemulsions and incorporate them in chitosan hydrogels to formulate a novel and possibly
142 more effective delivery system, the respective nanoemulsion-filled hydrogels. In both
143 systems, cannabidiol (CBD) was encapsulated as active ingredient of pharmacological interest.
144 Since the efficacy of the carrier and its ability to release and deliver the encapsulated bioactive
145 compound directly depends on its structure, the present study focuses on the structural study
146 of the developed systems in order to assess their suitability as delivery vehicles. In addition, a
147 biological evaluation was performed to assess the biocompatibility of the formulated
148 nanocarriers both in the presence and absence of CBD. Finally, the two systems under study
149 were compared in terms of release profiles and skin penetration potential of CBD to
150 determine their possible use as delivery vehicles for its the transdermal delivery.

151



152

Figure 1. Molecular structure of cannabidiol

153

154

155

156

157 **2. Materials and Methods**

158 **2.1. Materials**

159 Isopropyl tetradecanoate (IPM), 98% was purchased from Alpha Aesar, Germany.
160 Organic extra virgin olive oil (EVOO) from the Amfissa Variety, Pelion, Magnesia, Greece,
161 (acidity <0.4%, oleocanthal 124 mg/kg, oleacein 72 mg/kg, total hydroxytyrosol derivatives
162 140 mg/kg, total phenols 315 mg/kg) was a gift by “Myrolion” start-up company, Pelion,
163 Magnesia, Greece. Polyoxyethylenesorbitan monooleate (Tween 80), pure, was from Fisher
164 BioReagents, NH, USA. Glycerol monolinoleate (Maisine® CC) HLB 1, Caprylocaproyl Polyoxyl-
165 8 glycerides (Labrasol®) HLB 12 and Diethylene glycol monoethyl ether (Transcutol® HP) were
166 kindly donated by Gattefossé, France. Chitosan (200-600 mPa·s, 0.5% in 0.5% Acetic Acid at
167 20°C) was purchased from TCI, Belgium. CBD (99% of cannabidiol) from Cannabis sativa L. was
168 a gift from Ekati Alchemy Labs S.L, Barcelona, Spain. 5-Doxyl stearic acid (5-DSA) ammonium
169 salt, >99% purity, was from Avanti Polar Lipids, Alabama, USA. 12- Doxyl stearic acid (12-DSA)
170 was from Sigma-Aldrich Chemie GmbH Munich, Germany. Acetic Acid glacial 100% was from
171 Merck, Darmstadt, Germany. The porcine ears used as model membranes for the *ex vivo*
172 experiments conducted in the Faculty of Pharmacy, University of Belgrade, Belgrade, Serbia
173 were kindly gifted by a local provider. Ethanol absolute, analytical grade was purchased from
174 Fisher Scientific, Loughborough, UK. Deionized water was used.

176 **2.2. Formulation of nanoemulsions by low-energy method**

177 Low-energy O/W nanoemulsions (L1, L2) were prepared by the isothermal
178 spontaneous self-emulsification procedure [23] using water, a mixture of surfactants
179 (Labrasol, Tween 80, Maisine), and either IPM or a mixture of IPM with EVOO (1:1 mass ratio).
180 To formulate the nanoemulsions, an oily phase was initially prepared by mixing the surfactants
181 with the oil/oils using a magnetic stirrer. After mixing, the oily phase was slowly added into
182 the water under constant magnetic stirring at room temperature. The prepared
183 nanoemulsions were transferred to glass bottles and stored protected from light.

185 **2.3. Formulation of nanoemulsions by high-energy method**

186 High-energy O/W nanoemulsions (H1, H2) were prepared in a two-step emulsification
187 procedure [23] using water, cosolvent (Transcutol), mixtures of surfactants (Labrasol, Tween
188 80, Maisine) and a mixture of IPM and EVOO (1:1 mass ratio). Initially, coarse emulsions were
189 obtained with mechanical stirring at room temperature and then nanoemulsions were
190 formulated by passing the emulsions through a Panda PLUS1000 (GEA, Niro Soavi, Parma,

1
2
3
4
5
6
7
8
9
10
11
12
13
14
15
16
17
18
19
20
21
22
23
24
25
26
27
28
29
30
31
32
33
34
35
36
37
38
39
40
41
42
43
44
45
46
47
48
49
50
51
52
53
54
55
56
57
58
59
60
61
62
63
64
65

191 Italy) high-pressure homogenizer at max 390 bar applying up to 10 recirculation passages.
192 Nanoemulsions after their exit from the homogenizer were immediately cooled using an ice
193 bath.

194 The composition of the nanoemulsions is shown in Table 1.

195

196 *2.4. CBD-loaded nanoemulsions*

197 Initially, CBD was dissolved in the 1:1 mixture of IPM and EVOO to result stock
198 solutions at different concentrations. Then, CBD stock solution was mixed with the other
199 components to result O/W nanoemulsions as mentioned above. Final concentrations of CBD
200 in the nanoemulsions were from 1 mg/g to 10 mg/g of nanoemulsion.

201

202 *2.5. Formulation of nanoemulsion-filled hydrogels*

203 Chitosan hydrogels were formed in glass tubes by mixing chitosan flakes with 1%
204 acetic acid solution under gentle stirring using a spatula. Nanoemulsion-filled hydrogels were
205 formed by adding different amounts of O/W nanoemulsions to hydrogels prepared as
206 mentioned above. Nanoemulsions were incorporated by gentle stirring into the hydrogels
207 using a spatula.

208

209 *2.6. Dynamic light scattering (DLS) measurements*

210 Droplet size and droplet size distribution of empty and loaded O/W nanoemulsions
211 were measured by dynamic light scattering (DLS) using a Zetasizer Nano ZS (ZEN3600) analyser
212 (Malvern Instruments Ltd, Malvern, UK). The analyser was equipped with a He-Ne laser (633
213 nm) and Non-Invasive Backscatter (NIBS) optics. Measurements were carried out at 25 °C at a
214 scattering angle of 173 ° and processed using the Malvern Zetasizer Nano software, version
215 6.32 (Malvern Instruments Ltd, Malvern, UK). The cumulants' analysis gives two values, a
216 mean value for the size (Intensity mean) and a width parameter known as the polydispersity
217 index (Pdl). Samples were filtered through 0.45 µm hydrophilic PTFE filters (Millex-LCR from
218 Millipore Merck KGaA, Darmstadt, Germany) and contained in a quartz type cuvette under
219 dust-free conditions. Each sample was measured in triplicate. From these data were
220 calculated the mean and standard deviations.

221

222 *2.7. Stability studies*

223 Changes in mean droplet diameter and Pdl of empty and CBD-loaded O/W
224 nanoemulsions were investigated using the Zetasizer NanoZS device (ZEN3600) (Malvern

225 Instruments Ltd, Malvern, UK) as mentioned above. Measurements were conducted
226 immediately after preparation and again at given time intervals. Each sample was measured
227 in triplicate. Mean values and standard deviations were calculated from this data.

228

229 *2.8. Electron Paramagnetic Resonance (EPR) spectroscopy measurements*

230 EPR is a spectroscopic technique that measures the absorption of microwaves by
231 materials with unpaired electrons. Interactions of an unpaired electron with its environment
232 influence the shape of an EPR spectral line thus giving insight into dynamic processes such as
233 molecular motions or fluidity. In the present study, two doxyl stearic acid derivatives (5-DSA
234 ammonium salt and 12-DSA) labelled at different positions of the fatty acid aliphatic chain (C5
235 and C12) were used to study the fluidity and structure of the surfactants layer at different
236 depths.

237 EPR measurements were performed at room temperature with an EMX EPR
238 spectrometer (Bruker BioSpin GmbH, Germany) operating at the X-Band (9.8 GHz). A low
239 dielectric constant quartz flat cell for aqueous samples (Wilma-LabGlass, Cortecnet Europe,
240 France) was used to contain the O/W nanoemulsions and the corresponding nanoemulsion-
241 based hydrogels. Typical EPR settings were center field of 0.348 T, scan range 0.01 T, gain of
242 5.64×10^3 , time constant of 5.12 ms, conversion time of 5 ms, modulation amplitude of 0.4 mT.
243 Data collection and analysis were performed using the Bruker WinEPR acquisition and
244 processing program (Bruker BioSpin GmbH, Germany).

245 Sample preparation for EPR measurements was as follows: Initially 2 mM stock
246 solutions of the spin probes (5-DSA, 12-DSA) in ethanol were made. Then, appropriate
247 amounts of these concentrated solutions were inserted in eppendorf tubes. After ethanol
248 evaporation, 1 mL of the nanoemulsions was added. For the preparation of the corresponding
249 hybrid systems the aforementioned nanoemulsions were incorporated to hydrogels. Final
250 concentration of the spin probes was 0.02 mM.

251

252 *2.9. Small-angle X-ray scattering (SAXS) measurements*

253 Small angle X-ray Scattering (SAXS) experiments were carried out on a XEUSS 2.0
254 device (XENOCS, Grenoble, France). Coupled to a FOX 3D single reflection optical mirror
255 centered on the Cu K α radiation ($\lambda = 1.54 \text{ \AA}$), the GeniX 3D source delivers an 8 keV beam
256 which is collimated and defined by a set of 2 motorized scatterless slits. The samples were put
257 in thin glass capillaries (optical path 2 mm) which were then airtight sealed. The data were
258 collected by a two-dimensional PILATUS-300k detector (DECTRIS, Switzerland) placed at

1
2
3
4
5
6
7
8
9
10
11
12
13
14
15
16
17
18
19
20
21
22
23
24
25
26
27
28
29
30
31
32
33
34
35
36
37
38
39
40
41
42
43
44
45
46
47
48
49
50
51
52
53
54
55
56
57
58
59
60
61
62
63
64
65

259 different distances from the sample, giving access to the angle range $0.056^\circ - 2.26^\circ$ (0.04 nm^{-1}
260 $^1 - 1.6 \text{ nm}^{-1}$). A thermostatically controlled module makes it possible to carry out studies in T
261 from -30°C to 150°C . The measurements were performed at room temperature.

262

263 *2.10. Confocal Fluorescence Microscopy*

264 Confocal fluorescence microscopy was performed to detect and visualize the oil phase
265 of the nanoemulsions and the respective hybrid systems. For that reason, the oil phase (1:1
266 mixture of IPM/EVOO) was stained with the lipophilic dye Nile red. Then nanoemulsions and
267 the corresponding nanoemulsion-filled hydrogels were formulated as mentioned above (2.3
268 and 2.5) using the aforementioned oil phase. Following, one drop of the stained samples was
269 placed on a slide and covered with a cover slip, ensuring that there were no air bubbles.
270 Samples were mounted and visualized using a confocal laser scanning microscope (Leica TCS
271 SPE, Leica Microsystems, Heidelberg, Germany), with an excitation wavelength at 488 nm and
272 emission wavelength at 500 nm. For the images acquisition LAS AF software (Leica
273 Microsystems) was used.

274

275 *2.11. Cryo-Electron Microscopy*

276 The morphology of the CBD-loaded and empty nanoemulsion samples were studied
277 using cryogenic transmission electron microscopy method. For that purpose, quantifoil® R2/1
278 grids were utilized as a substrate. The grids were treated and prepared according to a well-
279 established protocol which is fully described elsewhere [36]. The grids were then loaded in a
280 ThermoFisher Scientific Vitrobot Mark IV grid plunger. The chamber of the grid plunger was
281 adjusted at 4°C and $>95\%$ relative humidity. A $3.5 \mu\text{L}$ aliquot from each sample were applied
282 on the prepared grids and blotted using type 595 filter paper for 6 seconds. The blotted grids
283 were plunged in liquified ethane were further assembled in autogrids and loaded inside the
284 ThermoFisher Scientific Glacios 200 kV CryoEM under cryogenic conditions. The micrographs
285 were acquired at the pixel size of $3.17 \text{ \AA}/\text{pixel}$ and $30 \text{ e}/\text{\AA}^2$ electron dose using ThermoFisher
286 Scientific EPU V 2.11 software.

287

288 *2.12 Cell Culture and Cell Proliferation Assay*

289 WS1 human normal skin fibroblasts were purchased from the American Type Culture
290 Collection (ATCC, Manassas, VA, USA). The cell line was grown in complete EMEM culture
291 medium (containing 2 mM L-glutamine, 1 mM sodium pyruvate, and 1500 mg/L sodium
292 bicarbonate), supplemented with 10% FBS and 1% penicillin/streptomycin (Gibco-Life

1
2
3
4
5
6
7
8
9
10
11
12
13
14
15
16
17
18
19
20
21
22
23
24
25
26
27
28
29
30
31
32
33
34
35
36
37
38
39
40
41
42
43
44
45
46
47
48
49
50
51
52
53
54
55
56
57
58
59
60
61
62
63
64
65

293 Technologies), at 37 °C in a humidified incubator with 5% CO₂. Cells were cultivated in 96 well
294 tissue culture plates (1.6×10^4 per well) and treated with different concentrations (0.5–1.75
295 mg/mL) of the formulated nanoemulsion and the respective nanoemulsion-filled hydrogel in
296 absence and presence of the bioactive compound for 72 h. Non-treated cells were used as
297 control.

298 Inhibition of cell proliferation was assessed 72 h after treatment by the MTT (3-(4,5-
299 Dimethyl-2-thiazolyl)-2,5-diphenyl-2H-tetrazolium bromide) assay according to the
300 manufacturer's standard protocol. To each culture being assayed MTT stock solution (5
301 mg/mL) was added to equal one tenth of the original culture volume and then incubated for
302 3 h. At the end of the incubation period the solution was discarded, and the converted dye
303 was solubilized in 1:1 isopropanol/DMSO solution to dilute the insoluble purple formazan
304 crystals. Absorbance of the converted dye was measured at 570 nm. Cell viability was
305 calculated using the equation below:

$$\text{Cell viability (\%)} = (\text{OD of treated cells}) / (\text{OD of control}) \times 100$$

308 where, OD is the optical density.

311 2.13. *In vitro* permeation study

312 In order to evaluate the skin permeation of CBD from the nanoemulsions and the
313 respective nanoemulsion-filled hydrogels an *in vitro* permeation protocol was implemented
314 using full-thickness porcine ear skin as the model membrane. The porcine ears were obtained
315 from a local slaughter house in Serbia and were processed appropriately. The porcine ears
316 were washed with cold tap water immediately after slaughter, dried carefully with soft tissue,
317 wrapped with aluminum foil and stored at –20 °C to be preserved as intact as possible until
318 use. Subsequently, for the implementation of the *in vitro* protocol, the porcine ears were
319 defrosted at room temperature and the hair were shortened carefully with electric trimmer
320 to obtain a sufficiently clear surface without destroying hair follicles or damage the stratum
321 corneum (SC). Then the full-thickness skin was detached from the cartilage using a scalpel and
322 punched with a custom-made spherical cutter of a 25 mm diameter to achieve the desired
323 discs used as membranes for the experiment. To ensure the integrity of the skin barrier trans-
324 epidermal water loss (TEWL) (Tewameter® TM 210; Courage+Khazaka, Köln, Germany) was
325 measured.

1 326 The full-thickness skin discs were placed on modified Franz diffusion cells with a surface
2 327 of 2.01 cm² and a receptor chamber of 12 mL volume (Gauer Glas, Germany) and the water-
3 328 bath temperature was set at a constant of 32 °C in agreement with the mean skin surface
4 329 temperature. To conduct the experiment the receptor compartments were filled with a
5 330 preheated mixture of PBS 1X solution and ethanol 96% V/V (1:1) which was under constant
6 331 stirring using a magnet at 500 rpm. The porcine full-thickness skin was placed between the
7 332 donor and receptor compartments with the SC towards the donor chamber. After 30 min of
8 333 equilibration, the donor compartments were uniformly filled with 0.5 mL of the formulations
9 334 (CBD-loaded nanoemulsions or nanoemulsion filled hydrogels) and covered with Parafilm® to
10 335 prevent evaporation. Samples of 500 µL volume were collected every 2 hours for a total of 30
11 336 hours of experiment starting from the formulation application. The receptor compartments
12 337 were filled again each time after sampling with an equal volume of fresh pre-warmed medium.
13 338 To determine the amount of CBD in the samples a LC-MS/MS method was used as described
14 339 below (paragraph 2.15). From the obtained results were determined the release profiles from
15 340 the two proposed nanocarriers and were calculated the steady-state flux (J_{ss}), cumulative
16 341 amount of CBD permeated through the skin at the end of the 30 h of the experiment (Q_{30h}),
17 342 and permeability coefficient (K_p) as described elsewhere [37].
18 343

31 344 2.14. Tape stripping experiments

32 345 The technique of tape stripping using porcine ear was implemented to evaluate the two
33 346 systems under study in terms of CBD penetration through the stratum corneum (SC) [38]. For
34 347 this experiment a porcine ear preserved as described above was initially thawed, and after
35 348 hairs were removed with a hair trimmer, it was fixed on Styrofoam plates without detaching
36 349 the skin from the cartilage. In order to determine the appropriate time point to apply the
37 350 formulation the TEWL was measured periodically using a Tewameter® TM 210 and when it
38 351 reached a value of approximately 15 g.m-2.h-2 [39] the CBD-loaded nanoemulsion and the
39 352 respective hybrid were cautiously applied on the marked skin sites. The study was conducted
40 353 under infinite dose regimen, using the same dosing conditions as for in vitro skin permeation
41 354 study (1 mL of each of the formulations were left on the skin for 2 h (effective diffusion area:
42 355 4.02 cm²)). To determine the amount of SC removed, each adhesive tape was weighted
43 356 accurately before starting the tape stripping. At the end of the 2 h incubation time, the excess
44 357 formulations were carefully removed using dry cotton swabs and the process of gradual
45 358 removal of the SC began, for which 30 adhesive D-squame® discs (CuDerm Corporation, USA)
46 359 were used. For this procedure the adhesive tapes were pressed onto the skin with a roller to
47
48
49
50
51
52
53
54
55
56
57
58
59
60
61
62
63
64
65

1
2
3
4
5
6
7
8
9
10
11
12
13
14
15
16
17
18
19
20
21
22
23
24
25
26
27
28
29
30
31
32
33
34
35
36
37
38
39
40
41
42
43
44
45
46
47
48
49
50
51
52
53
54
55
56
57
58
59
60
61
62
63
64
65

360 avoid any wrinkling and then were removed. After repeated weighing, each tape was inserted
361 into a centrifuge tube to extract the CBD. To achieve that, 4 ml of ethanol (70%, v/v) was
362 added in each tube and followed sonication (Sonorex RK 120H, Bandelin, Berlin, Germany) for
363 15 min and the centrifugation at 4000 rpm for 5 min (Centrifuge MPW-56; MPW Med.
364 Instruments, Warszawa, Poland). The final supernatant was collected and analysed for CBD
365 content using LC-MS/MS method [38].

366 367 2.15. LC-MS/MS method

368 Determination of CBD in aliquots obtained during in vitro penetration and permeation studies
369 was performed by using LC-MS/MS method. A liquid chromatographic system Accela 1000
370 (Thermo Fisher Scientific, San Jose, California, USA) consisting of an auto sampler and
371 quaternary pump was used. Chromatographic separation was achieved using Infinity Lab
372 Poroshell 120 EC-C18 (100 mm x 4.6 mm, 2.7 μ m; Agilent Technologies, USA) at 40 °C. Mixture
373 of acetonitrile and 0.1% formic acid (80:20, v/v) was used for isocratic elution at flow rate of
374 500 μ L/min. Total analysis time was 6 min. A TSQ Quantum Access MAX triple quadrupole
375 spectrometer was used mass analyses. The spectrometer was equipped with electrospray
376 ionization source and worked with nitrogen as nebulizing gas. ESI source parameters were
377 optimized by syringe infusion (20 μ L/min) of CBD standard solution. For data acquisition
378 selected reaction monitoring (SRM) positive scan mode was used. ESI source and mass
379 spectrometry parameters were as follows: spray voltage 3500 V; vaporizer temperature 400
380 °C; sheath gas pressure 50 units; ion sweep gas 0 units; auxiliary gas 45 units; ion transfer
381 capillary temperature 250 °C; capillary offset 35 units; tube lens offset 50 units; skimmer offset
382 0 units; peak width relating to resolution 0.7 for Q1; scan with (m/z) 0.02; scan time 200 ms.
383 Xcalibur software v. 2.1.0.1139 was used for data acquisition and processing (Thermo Fisher
384 Scientific, San Jose, CA, USA). Mass spectrometry was used for detecting specific ions for
385 analyte identification. MS full-scan mass spectra indicated that in ESI source [M+H]⁺ was the
386 dominant ion for CBD (m/z 315.3). The setting of SRM transition channel for CBD monitoring
387 was selected product ions at m/z 193.2 (collision energy was 19 V).

388 389 **3. Results and discussion**

390 *3.1. O/W nanoemulsions*

391 *3.1.1. Formulation of O/W nanoemulsions*

392 O/W nanoemulsions are thermodynamically metastable but kinetically stable nano-
393 sized emulsions, composed of oil droplets dispersed in an aqueous medium and stabilized by

394 surfactant molecules. Usually, for the formulation of nanoemulsions either high-energy or
 395 low-energy methods are applied. As can be seen in Table 1, low-energy O/W nanoemulsions
 396 were prepared with water as continuous phase, a 2:2:1 (mass ratio) mixture of Tween
 397 80/Labrasol/Maisine as surfactants and IPM as dispersed oil phase (L1). Following, low-energy
 398 nanoemulsions which contained water as continuous phase, the same blend of surfactants
 399 and a 1:1 mixture of IPM/EVOO as oil phase were formulated (L2). Both low energy
 400 nanoemulsions were opaque and remained visually stable for at least 80 days. When
 401 nanoemulsions having the same composition as L2 but homogenized by the two-step high-
 402 energy emulsification procedure were developed (H1), visual destabilization occurred 50 days
 403 after their formulation. High-energy nanoemulsions containing 1% Transcutol, a colorless
 404 liquid commonly used as cosolvent in many surfactant formulations, were formulated and
 405 remained visually stable for 60 days (H2).

406 In the present study, all nanoemulsions contained a 2:2:1 mixture of Tween 80,
 407 Labrasol and Maisine. These surfactants are biocompatible and non-ionic having hydrophilic
 408 lipophilic balance (HLB) values ranging from 1 to 15. As reported in a previous study the HLB
 409 value of the mixture of Tween 80/Labrasol/Maisine was calculated by adding values of the
 410 individual surfactants and was found 11 [40]. It is well established in the literature that mutual
 411 solubilisation of two immiscible liquids such as oil and water drastically increase when blends
 412 of surfactants with different HLB values are used [41,42].

413 Following their formulation, both low- and high-energy O/W nanoemulsions were
 414 studied using analytical techniques based on scattering, spectroscopy, and microscopy to
 415 investigate their structural characteristics in relation to their composition and preparation
 416 method.

417

418 **Table 1.** Composition of the nanoemulsions.

Ingredients (% w/w)	System			
	L1	L2	H1	H2
Water	91	91	91	90
Tween 80	2	2	2	2
Labrasol	2	2	2	2
Maisine	1	1	1	1
Transcutol	-	-	-	1
IPM	4	2	2	2
EVOO	-	2	2	2

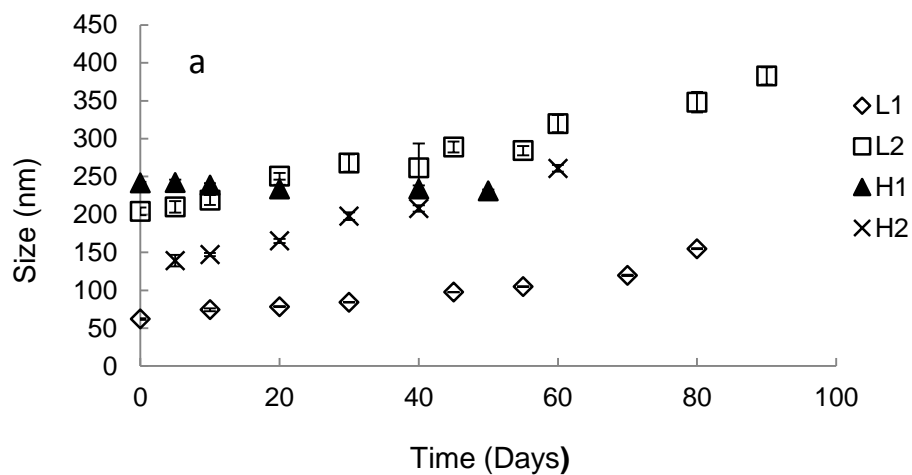
419

420

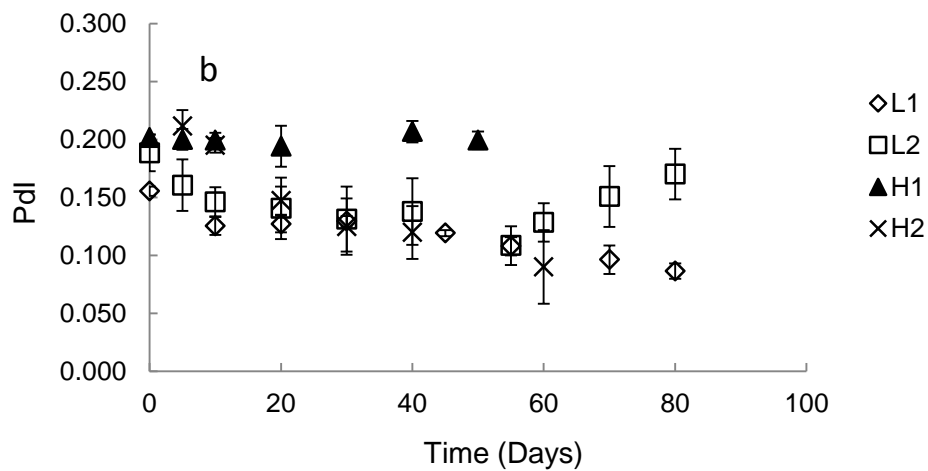
421

422 3.1.2. Droplet size, polydispersity index and stability

423 Dynamic light scattering (DLS) was applied to measure the hydrodynamic diameter of
424 the oil droplets and their size distribution. Measurements were taken immediately after
425 preparation and at given time intervals to evaluate storage stability of the samples. Figure 2
426 shows the variation of mean droplet diameter and Pdl with time for all nanoemulsions tested
427 (L1, L2, H1, H2). As can be seen in Fig 2a mean droplet diameter of L1 nanoemulsions increased
428 from 62 nm to 155 nm after a total of 80 days before phase separation. In the case of L2
429 nanoemulsions larger droplets were formulated probably due to the presence of EVOO in the
430 oil phase. Immediately after preparation mean diameter of the dispersed oil droplets was 204
431 nm. The size of the droplets was gradually increased up to 383 nm after 90 days of storage. In
432 the case of H1 nanoemulsions a small droplet size decrease from 242 nm to 231 nm within 50
433 days of storage was observed. Finally, when H2 nanoemulsions were examined, oil droplets
434 of 139 nm that increased up to 261 nm after 60 days of storage were obtained.



435



436

437 **Figure 2.** DLS study of O/W nanoemulsions: a) Droplet size and b) polydispersity index (Pdl) as
438 a function of time. (◇): L1; (□): L2; (▲): H1; (×): H2.

1
2
3
4
5
6
7
8
9
10
11
12
13
14
15
16
17
18
19
20
21
22
23
24
25
26
27
28
29
30
31
32
33
34
35
36
37
38
39
40
41
42
43
44
45
46
47
48
49
50
51
52
53
54
55
56
57
58
59
60
61
62
63
64
65

439 In Figure 2b, the polydispersity index is shown as a function of storage time. Both low-
440 and high energy nanoemulsions were monodispersed with Pdl <0.2. Similar findings have been
441 reported by our group in a previous study where O/W nanoemulsions containing 2% w/w of
442 the same oils but at different proportions and surfactant's mixture of HLB 11 were evaluated
443 [40].

444 In Figure 2 we can clearly observe that nanoemulsions containing EVOO in the oil
445 phase (L2, H1, H2) had larger oil droplets and higher Pdl as compared to the one composed of
446 IPM only (L1). EVOO is a mixture of triglycerides with a variety of minor components (mono-
447 and diacylglycerols, free fatty acids, phospholipids, sterols, tocopherols, polyphenols etc.) and
448 seems to affect both the size of the oil droplets and the physical stability of the final
449 formulation [43]. In general, the choice of the oil in terms of structure, polarity, surface
450 tension and viscosity has an important impact on the formulation of nanoemulsions. IPM is
451 an oil of lower viscosity as compared to EVOO generating nanoemulsions with smaller average
452 droplet size. On the other hand, oils of lower polarity such as vegetable oils are generally more
453 suitable regarding the physical stability of nanoemulsions, being less susceptible to Ostwald
454 ripening [44,45]. When the composition of the oil phase is complex, relative contribution of
455 each component to the final characteristics of the formulation must be considered.

456 To summarize, droplet size, size distribution, and stability of the O/W nanoemulsions
457 were affected by their composition and the emulsification procedure. Low energy
458 nanoemulsion in the absence of EVOO and Transcutol (L1) showed the lowest values of mean
459 droplet diameter and Pdl and remained stable for 80 days. When EVOO was added in the oil
460 phase mean droplet diameter was increased by several nanometres (L2, H1, H2). Besides, in
461 the presence of Transcutol (H2), smaller oil droplets as compared to L2, H1 were obtained
462 although these systems were destabilized 60 days after preparation. More specifically,
463 nanoemulsions with same composition but produced with different emulsification procedures
464 (L2, H1) exhibited differences in the stability measured in terms of hydrodynamic diameter
465 and polydispersity index (Pdl).

466 Considering the results of the DLS study regarding droplet size and stability,
467 nanoemulsions consisted of 91% w/w water, 2% w/w IPM, 2% w/w EVOO and 5% w/w blend
468 of surfactants (L2) were proved as more appropriate for the encapsulation of CBD. These
469 nanoemulsions are more advantageous than the other systems as encapsulation vehicles of
470 CBD since they contain EVOO, a natural vegetable oil with health benefits [46]. What is more,
471 L2 nanoemulsions are stabilized in the absence of cosolvent applying the low-energy

1
2
3
4
5
6
7
8
9
10
11
12
13
14
15
16
17
18
19
20
21
22
23
24
25
26
27
28
29
30
31
32
33
34
35
36
37
38
39
40
41
42
43
44
45
46
47
48
49
50
51
52
53
54
55
56
57
58
59
60
61
62
63
64
65

472 emulsification technique making them more promising as drug carriers in potential industrial
473 application.

474

475 *3.2. Encapsulation of CBD*

476 *3.2.1 Formulation of CBD-loaded nanoemulsions*

477 Cannabidiol (CBD), a naturally occurring cannabinoid, is a highly lipophilic
478 terpenophenolic compound. For its encapsulation in the oil droplets of O/W nanoemulsions a
479 procedure based on emulsification was applied as described in Methods (2.4. CBD-loaded
480 nanoemulsions). The effect of CBD encapsulation on droplet size, polydispersity, stability, and
481 membrane dynamics was evaluated using DLS, EPR and SAXS. For the DLS experiments CBD
482 concentration in the final nanoemulsions was 1 mg/g and 5 mg/g.

483

484 *3.2.2. Droplet size, polydispersity index and stability of CBD-loaded nanoemulsions*

485 As can be seen in Table 2, immediately after preparation, smaller oil droplets as
486 compared to empty L2 nanoemulsions were observed. The dispersion index PDI which reflects
487 the distribution of particle size, was below 0.25 showing uniform dispersions. In CBD loaded
488 nanoemulsions, oil droplets of 126 ± 3 nm diameter and 0.18 ± 0.01 PDI were formulated in the
489 presence of 1 mg/g CBD. When the concentration of the lipophilic active compound was
490 increased up to 5 mg/g, the size of the droplets was further decreased and the PDI increased
491 to 0.24 ± 0.01 . In both cases mean oil droplet diameter was increased with time while the PDI
492 was initially decreased and then remained practically unchanged and lower than 0.2. These
493 findings indicate that the presence of CBD in the oily droplets of the nanoemulsions influences
494 certain physicochemical characteristics and therefore further studies should be carried out to
495 elucidate the interplay between all components. In previous studies when encapsulation of
496 curcumin, vitamin D3, and ibuprofen in O/W nanoemulsions was considered, different effects
497 were observed depending on the nature of the added compound. More specifically,
498 encapsulation of vitamin D3 or curcumin in the dispersed oil phase of edible O/W
499 nanoemulsions caused an increase in the size of the oil droplets. This was related to the
500 interfacial location of both bioactive compounds and their effect on membrane dynamics in
501 terms of rigidity and order [47,48]. In another study, ibuprofen, a lipophilic drug, was
502 encapsulated in O/W nanoemulsions based on limonene and surfactants' mixture without
503 affecting droplet size or stability. In that case localization of the drug exclusively in the oil cores
504 was indicated and related to the strong lipophilic character of the added compound [49]. In a
505 recent study of Zhao et al., encapsulation of lycopene within O/W nanoemulsions using

506 lactoferrin and sesame oil resulted in droplet size increase and was related to the limited
 507 solubility of lycopene in oil [50].

508

509 **Table 2.** Droplet size (d, nm) and polydispersity index (Pdl) of CBD-loaded nanoemulsions. The
 510 final concentration of CBD was 1 mg/g and 5 mg/g of nanoemulsion. Temperature was 25 °C.
 511 Data expressed as the mean ± SD.

512

[CBD]		Time (days)						
		0	10	20	30	45	80	95
1 mg/g	Size (nm)	126±3	178±3	204±2	223±4	236±4	277±6	296±8
	Pdl	0.18±0.01	0.11±0.01	0.09±0.01	0.10±0.21	0.09±0.03	0.11±0.02	0.11±0.02
5 mg/g	Size (nm)	102±3	185±10	178±6	182±9	214±6	342±10	389±8
	Pdl	0.24±0.01	0.23±0.01	0.22±0.01	0.20±0.02	0.15±0.02	0.15±0.02	0.16±0.02

513

514 3.3. Nanoemulsion-filled hydrogels

515 Chitosan hydrogels are three dimensional networks of a natural polycationic
 516 copolymer that can absorb and retain large amounts of water. In general, hybrid hydrogels
 517 are networks of natural or synthetic polymers that incorporate proteins, peptides, or nano-
 518 and microstructures, interconnected via physical or chemical means, to yield materials with
 519 improved mechanical strength and expand their range of applications [51].

520 In recent years, different approaches were applied to develop nanoparticle hybrid
 521 hydrogels with varying nanoparticle types and varying hydrogel frameworks [52]. As reported
 522 by our group in an earlier study, hybrid hydrogel can be developed adding 1.25 % w/v chitosan
 523 in a 1:1 mixture of acetic acid solution/nanoemulsions under mild conditions [40]. This
 524 method of preparation could be more advantageous compared to other ones previously
 525 mentioned in the literature since it's simple and rapid [53]. These hybrids were used as carriers
 526 for the encapsulation and effective delivery/release of vitamin D3 and curcumin. In the
 527 present study, the nanoemulsions used for the development of chitosan hybrid hydrogels
 528 were formulated with the low-energy homogenization procedure and consisted of 91% w/w
 529 water, 2% w/w IPM, 2% EVOO and 5% w/w surfactants' mixture (L2). For the encapsulation of
 530 CBD in hydrogels, nanoemulsions loaded with CBD were initially formulated as described in
 531 Methods (2.2.1. Preparation of nanoemulsions). These loaded nanoemulsions were then
 532 mixed with acetic acid 1% and chitosan as mentioned above to result the nanoemulsions-

533 based hydrogels. The concentration of CBD in the nanoemulsion-based hydrogels was 2.5
534 mg/mL.

535

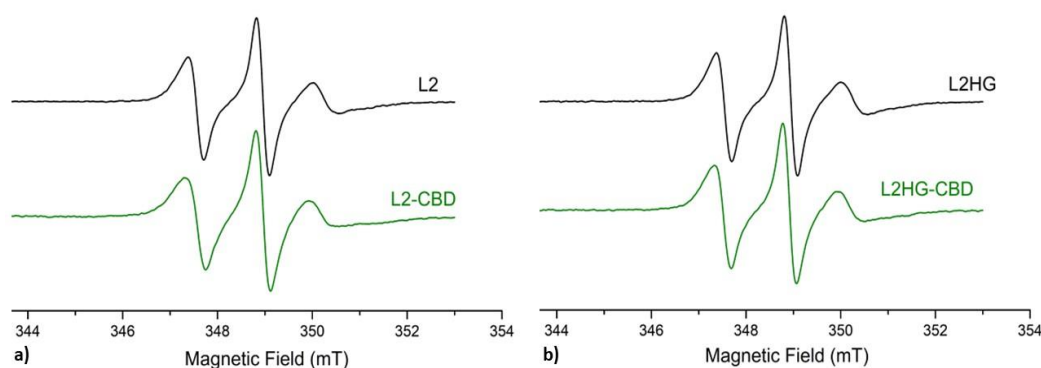
536 3.4. Dynamics of the surfactant layer

537 3.4.1. O/W nanoemulsions

538 EPR experiments using 5-DSA ammonium salt and 12-DSA as amphiphilic spin probes
539 were conducted to investigate the effect of the presence of CBD on local viscosity, order and
540 local polarity of the surfactants' layer in the O/W nanoemulsions. These probes are spin-
541 labelled fatty acid analogues consisting of stearic acid and an N-O• moiety attached to the C-
542 5 and C-12 position of the hydrocarbon chain, respectively. In the case of 5-DSA the
543 paramagnetic moiety of the probe is localized closer to the polar head groups of the
544 surfactants while in the case of 12-DSA it is localized closer to the surfactant tails. In other
545 words, 5-DSA senses variations closer to the aqueous phase whereas 12-DSA senses changes
546 of the oil phase that penetrates the lipophilic surfactant chains [54].

547 Figure 3 shows the experimental EPR spectra of 5-DSA ammonium salt in empty and
548 CBD-loaded O/W nanoemulsions and nanoemulsions-filled hybrid hydrogels. Three-line EPR
549 spectra of unequal heights and widths characteristic of doxyl derivatives when located in
550 membranes, were obtained in all cases.

551



552

553 **Figure 3.** EPR spectra of 5-DSA ammonium salt in (a) empty (L2) and full, CBD-loaded (L2-CBD)
554 O/W nanoemulsions and (b) empty (L2HG) and full, CBD-loaded (L2HG-CBD).

555

1
2
3
4
5
6
7
8
9
10
11
12
13
14
15
16
17
18
19
20
21
22
23
24
25
26
27
28
29
30
31
32
33
34
35
36
37
38
39
40
41
42
43
44
45
46
47
48
49
50
51
52
53
54
55
56
57
58
59
60
61
62
63
64
65

556 In Table 3, three parameters (τ_R , S and α_N) obtained from the EPR spectral
557 characteristics in the absence and the presence of CBD are presented. The detailed equations
558 and the physical meaning of those parameters have been reported in previous studies [55,56].
559 As can be observed, in the case of 5-DSA, both τ_R and S values were increased upon CBD
560 encapsulation in the oil phase of the O/W nanoemulsions. More specifically, τ_R was increased
561 from 2.5 ± 0.1 ns to 3.2 ± 0.1 ns and S from 0.13 ± 0.01 to 0.19 ± 0.01 (Table 3). The increase
562 of rotational correlation time (τ_R) in the presence of the bioactive compound is indicative of a
563 more hindered motion of the spin probe in the area close to the surfactants' polar head
564 groups. In addition, order parameter of the surfactants' layer was also increased showing a
565 more rigid environment in the same area. These changes indicate penetration and interaction
566 of CBD with the surfactant molecules rendering the surfactants' monolayer more viscous and
567 less flexible. The nitrogen hyperfine splitting, α_N , of the N-O \cdot moiety of 5-DSA is a local polarity
568 parameter which remained practically the same in the presence of CBD. Similar findings were
569 recorded when the other spin probe, 12-DSA, was considered. In that case, τ_R and S values
570 were lower as compared to those of 5-DSA which could be explained by the different location
571 of 12-DSA in the membrane. The nitrogen hyperfine splitting, α_N , of the N-O \cdot moiety of 12-
572 DSA was higher both in the presence and absence of CBD, indicating differences in the micro
573 polarity at different depths of the surfactants' monolayer. Similar findings have been reported
574 in previous studies of our group when encapsulation of lipophilic compounds such as Vitamin
575 D3 in food grade O/W nanoemulsions [47] or extra virgin olive oil-in-water nanoemulsions
576 [48] were considered. Encapsulation of curcumin in O/W nanoemulsions containing
577 eucalyptol (EUC) or pinene in the dispersed oil phase also affected the surfactants layer
578 increasing local viscosity [57].

579 580 *3.4.2. Nanoemulsion-filled hydrogels*

581 Nanoemulsion-filled hybrid hydrogels were investigated by EPR spin probing
582 spectroscopy applying 5-DSA ammonium salt and 12-DSA. These amphiphilic spin probes were
583 used to monitor possible changes in the surfactants' layer after incorporation of the O/W
584 nanoemulsions into the chitosan hydrogels. As can be observed, membrane dynamics in
585 nanoemulsion-filled hydrogels as expressed by τ_R , S and α_N were similar to the corresponding
586 nanoemulsions showing that chitosan used as gelling agent at a concentration of 1.25 % w/v
587 has no effect on local viscosity, order and polarity. On the other hand, hydrogels were less
588 affected by the presence of CBD. More specifically, rotational correlation time (τ_R) was slightly
589 increased but order parameter (S) and local polarity remained the same.

590 **Table 3.** Rotational correlation time (τ_R), order parameter (S) and isotropic hyperfine splitting
 591 constant (α_N) of 5-DSA and 12-DSA in empty and loaded nanoemulsions (L1, L1-CBD) and
 592 hybrid hydrogels (L1HG, L1HG-CBD).

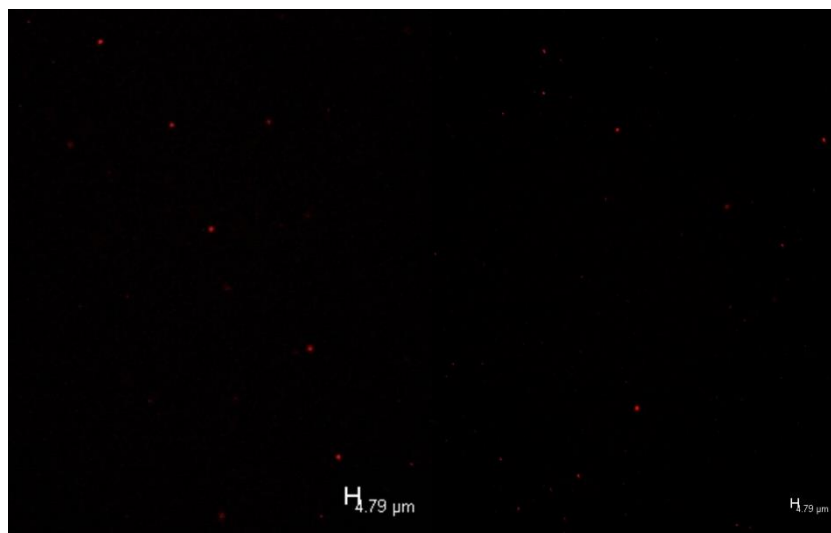
System	5-DSA			12-DSA		
	τ_R (ns)	S	α_N ($\times 10^{-4}$ T)	τ_R (ns)	S	α_N ($\times 10^{-4}$ T)
L1	2.5 \pm 0.1	0.13 \pm 0.01	13.8 \pm 0.0	1.4 \pm 0.0	0.08 \pm 0.00	14.4 \pm 0.0
L1-CBD	3.2 \pm 0.1	0.19 \pm 0.01	13.5 \pm 0.0	2.3 \pm 0.1	0.14 \pm 0.01	14.0 \pm 0.1
L1HG	2.4 \pm 0.2	0.15 \pm 0.02	13.5 \pm 0.1	1.5 \pm 0.1	0.09 \pm 0.01	14.4 \pm 0.1
L1HG-CBD	2.7 \pm 0.1	0.15 \pm 0.02	13.6 \pm 0.1	1.6 \pm 0.0	0.09 \pm 0.00	14.3 \pm 0.1

593

594 3.5. Confocal Microscopy

595 Confocal microscopy was implemented to determine the structure of the formulated
 596 systems and identify possible changes in the shape of the oil droplets after incorporation in
 597 the chitosan hydrogels. The fluorescent confocal microscopy images indicated that the oil
 598 droplets of the O/W nanoemulsions were spherical in shape and about 120 nm in diameter
 599 (Figure 4). Moreover, confocal micrographs obtained for the nanoemulsion-filled hydrogels
 600 (hybrids) show no significant changes in the shape or size of the incorporated nanoemulsions
 601 (Figure 4). Similar microscopy studies of both initial O/W nanoemulsions and the
 602 corresponding hydrogels have not been so far reported in the literature. In a study of
 603 McClements and co-workers, confocal microscopy images of O/W nanoemulsions containing
 604 Vitamin D3 and prepared using natural surfactants and different carrier oils indicated the
 605 presence of spherical nanodroplets [58]. In another study, confocal fluorescence microscopy
 606 was used to study the morphology of soluble hydrogels formulated with flavour oil
 607 nanoemulsions and biopolymers. Confocal micrographs of the systems under different
 608 conditions were obtained showing visible red structures of oil stained with Nile red [59].

609



610

611 **Figure 4.** Images of the Nile red- stained oil mixture of the formulated nanoemulsion (left) and
612 nanoemulsion-based hydrogels (right) obtained by confocal fluorescence microscopy (X 40
613 magnification).

614

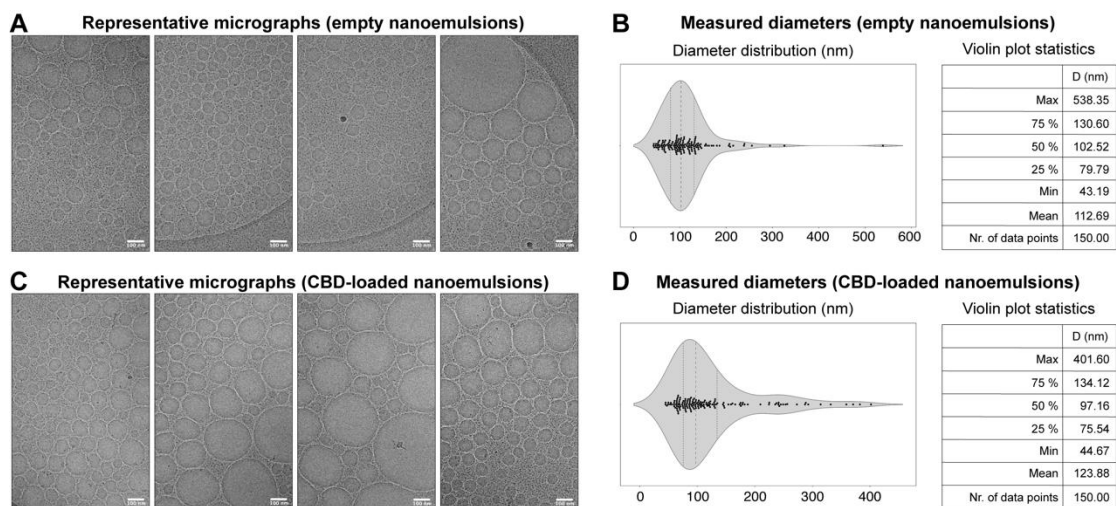
615 3.6. Cryo-Electron Microscopy

616 To directly observe the architecture of nanoemulsions and their CBD-loaded
617 conformation utilizing cryogenic electron microscopy (cryo-EM), all specimens were vitrified
618 by plunge-freezing (Materials and Methods). Nanoemulsions are cooled rapidly ($10^5 \text{ }^\circ\text{C s}^{-1}$) to
619 avoid ice crystal formation that perturbs their structure, producing, therefore, vitreous ice
620 that is amorphous similar to a liquid with high density. Due to nanoemulsions' high viscosity,
621 formation of vitreous ice was challenging as it is majorly affected by the intrinsic sample
622 viscosity that must be kept to a bare minimum [60]. Despite above-mentioned challenges, we
623 systematically probed vitrification conditions for all specimens and retrieved cryo-EM data for
624 the L2 nanoemulsions (Table 1) that eventually allowed direct observation of the content in
625 both unloaded and CBD-loaded states (Figure 5). This result shows that nanoemulsion
626 samples are in principle amenable to cryo-EM analysis.

627 Empty O/W nanoemulsions localized in thick vitreous ice regions, systematically
628 forming spherical signatures (Figure 5A). L2 nanoemulsions had preferential distribution in
629 thicker vitreous ice like polymersomes previously observed with cryo-EM [61–63] and
630 contrasts with the intrinsic surface properties of (proteo)liposomes that are frequently
631 observed on the amorphous holey carbon grid edge [64,65]. Indeed, as DLS data suggest
632 (Figure 2) their diameters slightly vary; due to their high sphericity, cryo-EM and DLS data
633 regarding diameters agree well (Figure 5B, Figure 2). We also characterized via cryo-EM rare
634 nanoemulsions with substantially larger diameters (Figure 5B) that may well serve for delivery

635 of more complex material in terms of size. CBD-loaded nanoemulsions exhibited similar
 636 architectural properties (Figure 5C) and statistical analysis of their particle diameters did not
 637 show any substantial change in their observed shapes (Figure 5D). This result suggests that
 638 CBD, which is encapsulated in those nanoemulsions (Figure 3) does not have observable
 639 effects on their structural rigidity and ultrastructure, suggesting minimal perturbations upon
 640 drug encapsulation.

641



642

643 **Figure 5.** Cryo-EM study of L2 nanoemulsions. (A) Representative micrographs of empty
 644 nanoemulsions showing their distribution, which is regulated by ice thickness (the thicker the
 645 ice, the highest the odds to identify the particles). Background black dots identified in the
 646 micrographs represent possible surfactants. (B) Violin plot illustrating the measurements of
 647 diameters for 150 single-particle nanoemulsions along with the underlying statistics in the
 648 accompanying table. Note the dots in the violin plots represents each single data point. (C)
 649 Same as (A), but for drug-loaded full nanoemulsions. (D) is same as (C), but for drug-loaded
 650 nanoemulsions.

651

652 3.7 Small angle X-ray Scattering (SAXS)

653 SAXS is an analytical and non-destructive method implemented for the investigation
 654 of nanostructures in liquids and solids. SAXS is able to probe the colloidal length scales of 10–
 655 1000 Å thus being a suitable tool for the determination of the size and the structure of
 656 colloidal systems such as microemulsions, nanoemulsions and hydrogels [66]. Actually,
 657 reaching the upper limit requires specific equipment and favourable systems. In the present
 658 study this method was initially implemented to determine the effect on the size when
 659 different concentrations of CBD were encapsulated in the nanoemulsions. Specifically, Figure
 660 6a, represents the intensity profile of the formulated nanoemulsions in absence and in

1
2
3
4
5
6
7
8
9
10
11
12
13
14
15
16
17
18
19
20
21
22
23
24
25
26
27
28
29
30
31
32
33
34
35
36
37
38
39
40
41
42
43
44
45
46
47
48
49
50
51
52
53
54
55
56
57
58
59
60
61
62
63
64
65
661 presence of various concentrations of CBD in the so-called Porod representation. Since
662 characteristic sizes are quite large, the scattering intensity I is dominated by the asymptotic
663 power-law decay $1/q^4$, also known as Porod's law, in the investigated scattering wave vector
664 q range. The Porod representation, namely $I \times q^4$ vs. q , magnifies deviations from Porod's law,
665 unravelling the structure [67].

666 Another practical limitation nevertheless comes here from the low contrast of organic
667 matter with respect to water and the ensuing low signal-to-noise ratio. Some firm structural
668 information still emerges from the processed data, at least in a semi-quantitative sense. The
669 depicted spectra in combination with the simulation (red line) provide an indication of the
670 structure of the nanoemulsions. First of all, the below spectra illustrate an oscillating red curve
671 simulating the scattering by an assembly of non-interacting, identical spheres with radius
672 about 49.3 nm, suggesting that the spherical model invoked in DLS and confocal microscopy
673 is structurally relevant also in SAXS for all the samples.

674 Then, the encapsulation of two different CBD concentrations, namely 1 mg/g and 5
675 mg/g, was investigated and compared with the respective nanoemulsions in absence of the
676 bioactive compound. It was observed that that the (truncated) «peak» around 0.0045 \AA^{-1} for
677 the CBD-free system moves to a slightly larger value, ca. 0.005 \AA^{-1} with CBD concentration
678 which should be associated with the decrease of the droplet size of the nanoemulsions with
679 the encapsulation of CBD. However, size is not significantly affected by concentration for the
680 two CBD-loaded systems. In contrast with the light scattering data, size remains unchanged
681 for both the CBD-loaded nanoemulsions indicating that the concentration of the encapsulated
682 compound does not affect the size of the formulated nanoemulsions.

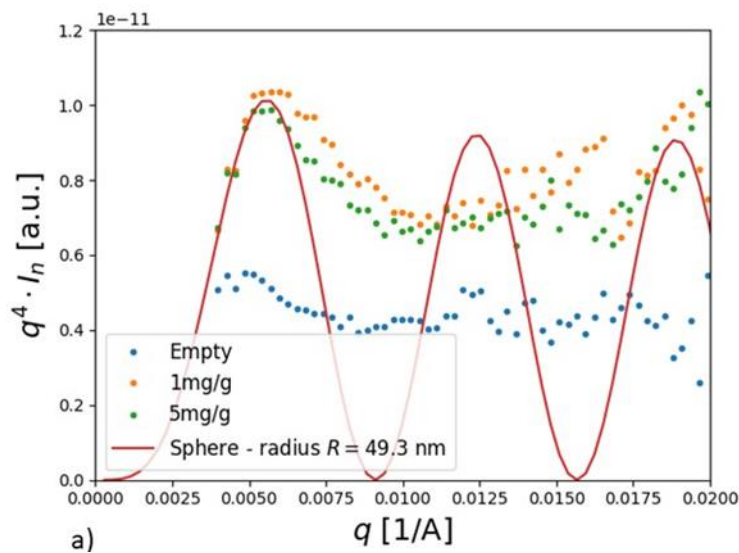
683 On the other hand, as may be observed from the SAXS curves (Figure 6a) the diameter
684 of the oil nanodroplets calculated by fitting SAXS data were always smaller than the values
685 measured by DLS (Figure 2 and Table 2). This was expected since DLS measures the hydration
686 layer that moves with the nanodroplets and not only droplet's size [68].

687 In addition, the structure of the chitosan hydrogel and the size of the nanoemulsions
688 after their incorporation in the hydrogels were studied to determine possible changes. First,
689 the chitosan hydrogel was examined and as can be seen from the spectrum presented in
690 Figure 6c two-dimensional (thin, with large lateral dimensions) objects like platelets may
691 describe the structure of the chitosan hydrogel. This hypothesis arises by the fact from the
692 $1/q^2$ intensity decay at large wave vectors. Consequently, nanoemulsions both in absence and
693 in presence of CBD were incorporated in the chitosan hydrogel resulting in the hybrid systems.
694 In Figure 6b are depicted the hybrid systems in absence of CBD and the CBD loaded hybrid

695 systems with CBD concentration 0.5 mg/g and 2.5 mg/g. These systems were also studied in
 696 terms of structure and size. The spectrum illustrated in Figure 6b demonstrates that the
 697 spherical structure and the size of the nanoemulsions were not affected by their incorporation
 698 in the hydrogel, with the CBD-free system again exhibiting a larger characteristic size than
 699 both CBD-loaded systems.

700 To summarize, the results obtained by the SAXS complete those acquired by EPR and
 701 confocal microscopy suggesting that indeed the incorporation of the nanoemulsions in the
 702 chitosan-based hydrogel could provide protection to the nanoemulsions without affecting
 703 significantly their structural properties.

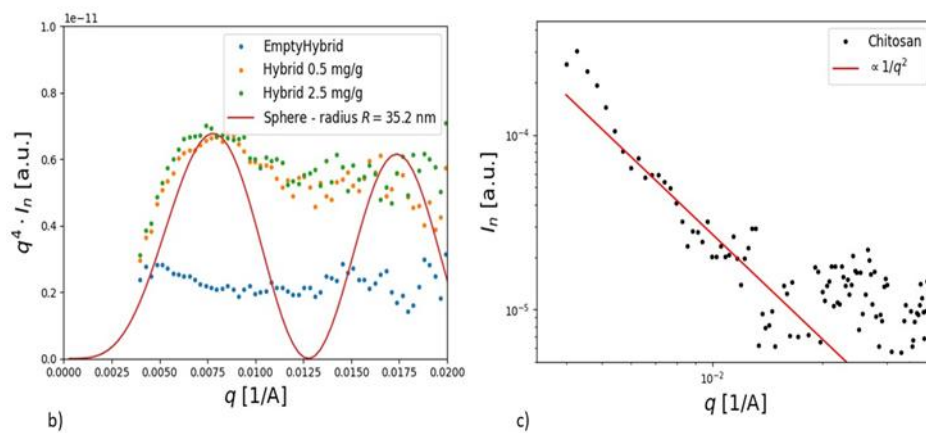
704



705

706

707



708

709 **Figure 6.** a) Data of SAXS in the Porod representation for empty and loaded nanoemulsions

710 Empty nanoemulsion (blue ●) and loaded systems with 1 mg/g CBD (orange ●) and 5 mg/g

1
2
3
4
5
6
7
8
9
10
11
12
13
14
15
16
17
18
19
20
21
22
23
24
25
26
27
28
29
30
31
32
33
34
35
36
37
38
39
40
41
42
43
44
45
46
47
48
49
50
51
52
53
54
55
56
57
58
59
60
61
62
63
64
65

711 CBD (green ●), simulation (red line). b) Empty nanoemulsion-filled hydrogel (blue ●) and
712 loaded systems with 0.5 mg/g CBD (orange ●) and 2.5 mg/g CBD (green ●), simulation (red
713 line). c) Chitosan hydrogel (black ●), simulation (red line).

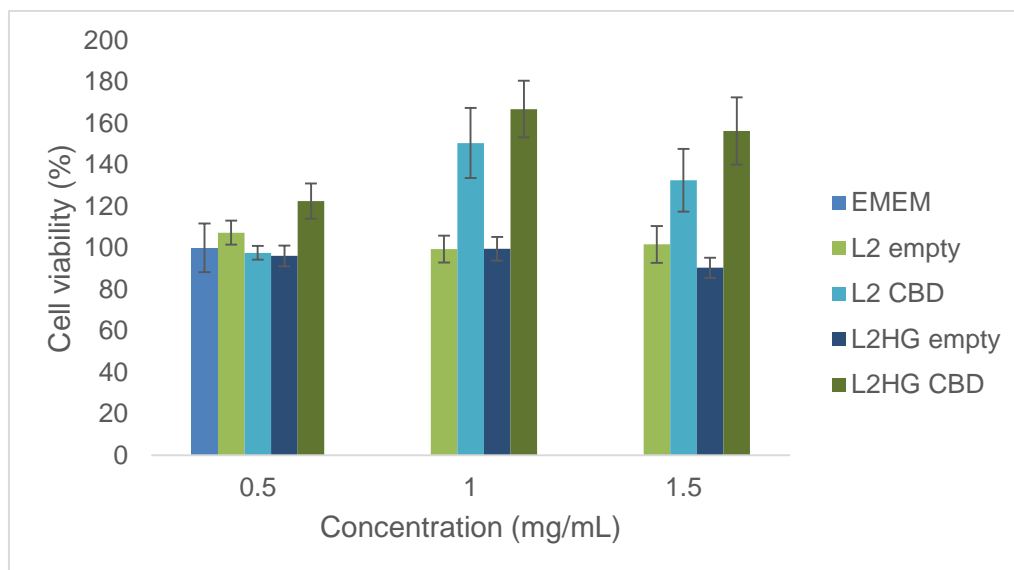
714

715 3.8 Cell viability

716 The suitability of a nanodispersion to be used as an effective carrier of bioactive
717 compounds depends on various factors. Biocompatibility of the nanocarrier itself, in absence
718 of the bioactive compound, is one of the most crucial factors. For that reason, the potential
719 skin irritation and cytotoxic effect of the formulated nanoemulsions and the respective
720 nanoemulsion-filled hydrogels were investigated *in vitro*. Following, the CBD-loaded systems
721 were also studied to evaluate the effects of the bioactive compound on the cell viability.
722 Cytotoxicity was assessed through the colorimetric MTT assay. This tetrazolium-based assay
723 measures the reduction of tetrazolium salt by intracellular dehydrogenases of viable living
724 cells. Since the formulated systems are intended for topical use and possibly for wound
725 healing, human normal fibroblasts (WS1) were used in order to compare the biocompatibility
726 of the two nanodispersions. Thus, WS1 cells were treated with the nanoemulsions and the
727 corresponding hydrogels in the absence and presence of CBD at a concentration range of 0.5
728 to 1.5 mg/mL in the culture medium. As can be seen in Figure 7, both the NEs and the NE/HGs
729 did not exhibit any cytotoxic effect up to the concentration threshold of 1.5 mg/mL in the cell
730 culture medium. The high biocompatibility of these systems could be attributed to the low
731 concentration of surfactants. In fact, there are indications that the administration of the
732 empty systems causes a dose-dependent induction of cell proliferation. This result could be
733 attributed to the use of olive oil in the oil phase [69,70] and the chitosan. As has been reported
734 before by Howling et al. [71], highly deacetylated chitosan, like the one used in our case,
735 strongly stimulated fibroblast proliferation. The exact mechanism of action has not been
736 elucidated however it is suggested that chitosan binds to serum factors, such as growth factors
737 [72]. Furthermore, at higher concentrations the CBD-loaded systems result in an increase of
738 cell viability indicating that CBD could also promote the proliferation of fibroblasts. Since until
739 recently, CBD was most commonly administered orally, there is no previous literature
740 evaluating the effect of CBD on normal human fibroblasts. However, there are indications that
741 the endocannabinoid system is involved in the wound healing response in fibroblast cells
742 through the upregulation of epidermal growth factors based on studies carried out using
743 murine models [4]. Furthermore, a recent *in vivo* evaluation of the CBD effect on the wound
744 healing process using rats demonstrated a noticeable regeneration of epidermis and dermis

745 [73]. Hence, the observed fibroblast proliferation when treated with the CBD-loaded systems
746 could be interpreted by the aforementioned studies. However, at the minimum concentration
747 administered (0.5 mg/mL) this effect is not evident and the systems under study did not
748 demonstrate significant different cell viability values. Recently, a similar cytotoxicity study was
749 described by Nigro et al. concerning the evaluation of fibroblasts cell viability after the
750 administration of nanoemulsion-filled hydrogels intended for topical administration of
751 coenzyme Q10 (coQ10) [74]. The specific research group demonstrated cell viability below
752 50% when the system in the absence of coQ10 was administered in concentration 1.25
753 mg/mL.

754 To conclude, the cell viability evaluation indicates that the nanodispersions under
755 study present high biocompatibility and could stimulate skin fibroblast proliferation. Hence,
756 these systems could be ideal candidates to be used as carriers for bioactive compounds with
757 antimicrobial and anti-inflammatory properties for the development of a novel wound healing
758 formulation.



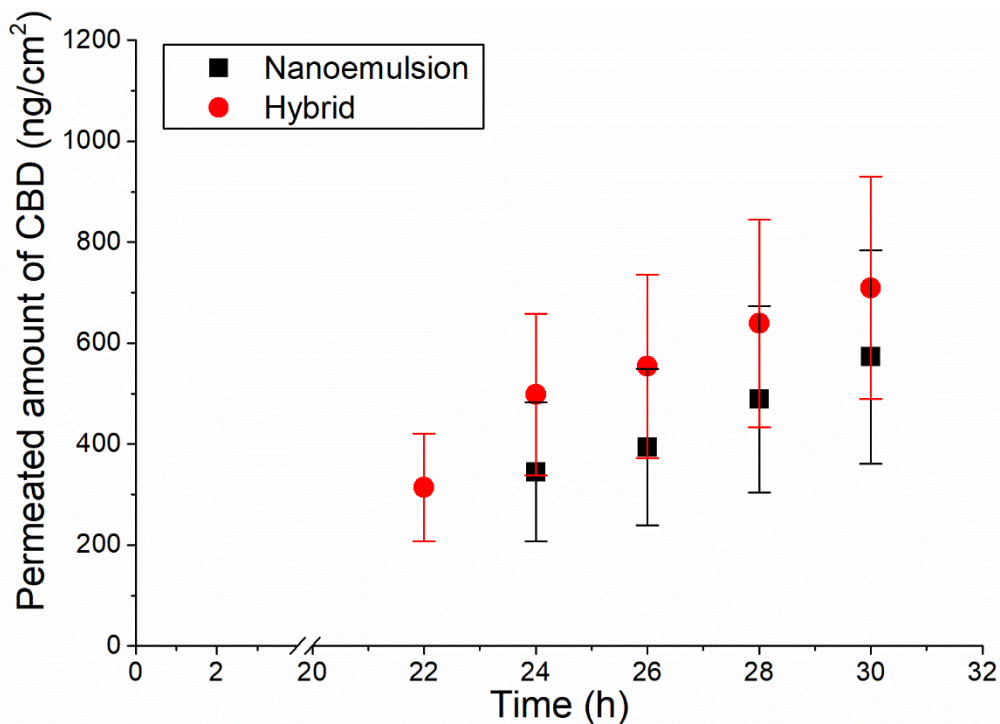
762 **Figure 7.** Cell viability testing results in WS1 human fibroblasts cell line after 72 h of treatment
763 with L2 nanoemulsion and the respective L2/HG nanoemulsion-filled hydrogel in the absence
764 and presence of CBD using the MTT cell proliferation assay. Each column represents the mean
765 of five replicates \pm SD.

769 3.9. In vitro permeation study

1
2
3
4
5
6
7
8
9
10
11
12
13
14
15
16
17
18
19
20
21
22
23
24
25
26
27
28
29
30
31
32
33
34
35
36
37
38
39
40
41
42
43
44
45
46
47
48
49
50
51
52
53
54
55
56
57
58
59
60
61
62
63
64
65

771 The evaluation of in vitro drug permeation from a carrier is a valuable tool since it provides
772 an indication concerning the bioavailability of the compound of interest and the suitability of
773 the formulated nanocarrier as a delivery vehicle. The effective release of a bioactive
774 compound as well as its diffusion through the skin are essential in order to obtain the desired
775 biological effects. In the present study the aim was to compare two different nanocarriers
776 namely the nanoemulsions (NE) and the respective nanoemulsion-filled hydrogels (NE/HG) as
777 delivery vehicles of cannabidiol (CBD) since the structural difference of these two formulations
778 could be expected to have impact on their ability to release and deliver the bioactive
779 substance into/through the skin [75]. In spite the fact that in vitro release studies using
780 synthetic membranes are very popular due to the ease of application, more than often the
781 obtained results cannot correlate with the in vivo performance or cannot detect possible
782 differences in release due to different structure [76]. For that reason, in the present study the
783 described in vitro permeation protocol was implemented using modified Franz diffusion cells
784 and full-thickness porcine ear skin as the model membrane. The experiment was conducted
785 under infinite dose regiment despite the fact that the amount of applied formulation is
786 significantly higher than the actual amount applied by patients. The infinite dose experiments
787 are selected since they allow to determine the maximum flux of the CBD from a formulation
788 and therefore enable to parametrically compare investigated formulations.

789 The amount of CBD permeated through the full-thickness porcine ear skin in function of
790 time is depicted in figure 8 Interestingly, no CBD has permeated through the porcine skin at
791 the beginning of the test as can be observed by the diagram in figure 8. Specifically, CBD was
792 initially detected in the acceptor compartment after the 24th and 22nd hours of
793 administration of the NE and the NE/HG, respectively. Before these time points, CBD
794 concentration was below the LC/MS-MS quantification limit. In the later sampling time points,
795 a higher permeation of CBD was observed from NE/HG compared to NE. In this regard, it is
796 important to emphasize that donor compartments were covered with Parafilm® in order to
797 prevent an extensive evaporation of water from the formulations during 30 h.



799

800 Figure 8. Ex vivo permeation profiles of cannabidiol (CBD) determined across the full-thickness
 801 pig ear skin (mean \pm SD, n=6) reflecting the influence of differences in nanocarrier type on the
 802 ex vivo skin absorption of CBD.

803

804 As presented in table 4. the hybrid systems demonstrated higher permeation rate and
 805 permeation coefficient which provides an indication of enhanced transdermal absorption. By
 806 the end of the 30 h incubation time, the cumulative amount of CBD that was detected in the
 807 acceptor compartment of the cells where hybrids were applied was also higher compared to
 808 the NE ones.

809

810 Table 4. Ex vivo skin penetration data for the different investigated colloidal systems after 30
 811 h of application (mean \pm SD, n=6).

	steady-state flux ($\mu\text{g}/\text{cm}^2\text{h}^{-1}$)	$Q_{30\text{h}}$ Cumulative amount of CBD permeated through the skin ($\mu\text{g}/\text{cm}$)	Permeation coefficient ($\text{mg}/\text{cm}^2\text{h}$)
Nanoemulsions	403.37 \pm 130.09	572.56 \pm 211.11	80.67 \pm 211.11
Hybrids	475.68 \pm 162.57	709.22 \pm 220.62	95.14 \pm 32.51

812

813

814 These results are expected since it is well-known that chitosan acts as penetration
 815 enhancer due to its interaction with the SC in various ways including the modification of the

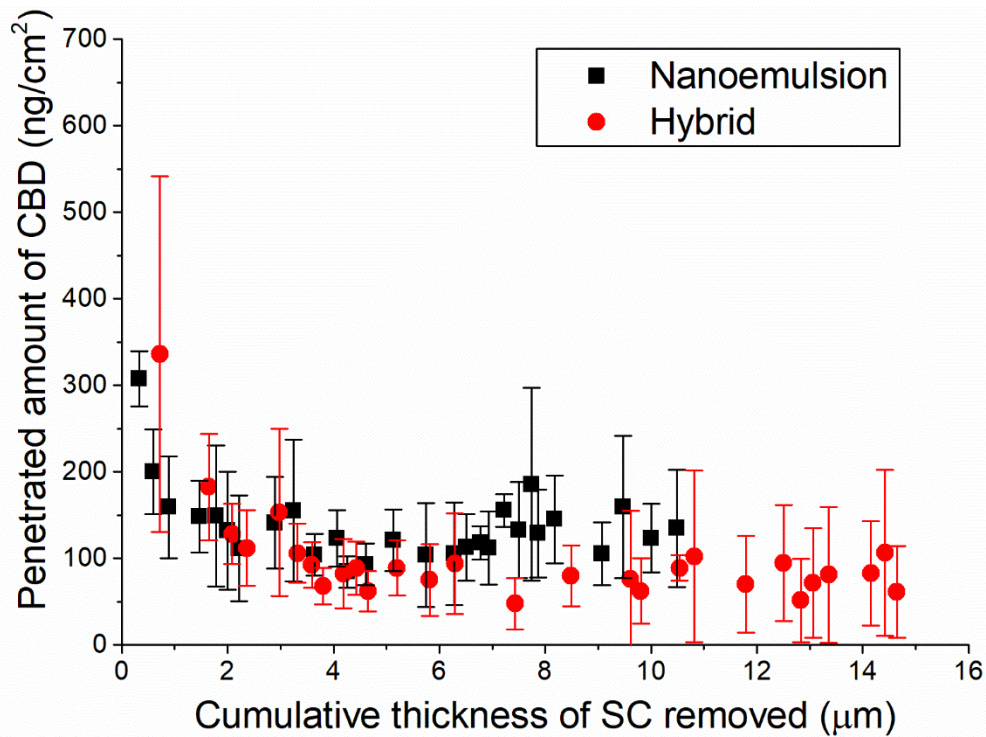
1
2
3
4
5
6
7
8
9
10
11
12
13
14
15
16
17
18
19
20
21
22
23
24
25
26
27
28
29
30
31
32
33
34
35
36
37
38
39
40
41
42
43
44
45
46
47
48
49
50
51
52
53
54
55
56
57
58
59
60
61
62
63
64
65

816 protein structure of the SC and acting as a moisturizing agent increasing the SCs' water content
817 [77–79]. In addition, skin occlusion also enhances the percutaneous absorption, especially for
818 very lipophilic substances such as CBD [80]. This effect is proportional to the duration of
819 occlusion hence the penetration of the bioactive compounds is enhanced with increasing
820 duration of occlusion [81]. Skin occlusion leads to increased skin hydration, while extended
821 skin hydration (> 8h) causes a swelling of corneocytes, creating inter-corneocyte ruptures, and
822 causes microstructural changes in lipid self-assembly, leading to changes in skin barrier
823 properties [82–84].
824 Therefore, the obtained results indicated that the NE/HG itself contributed to the improved
825 penetration of CBD. However, it is important to emphasize that no statistically significant
826 difference was found regarding monitored permeation parameters, probably due to high
827 variability of obtained results. The high variation is highly expected and is frequently reported
828 in the literature, since porcine ear skin was used as the biological membrane. It is well known
829 that it is difficult to control the breeding and diet conditions of pigs, which can affect, inter
830 alia, the skin properties (the ears are obtained from local abattoir immediately after
831 slaughter).

832 833 3.10. Tape stripping experiments

834 As aforementioned the presence of chitosan in the proposed NE/HG used in permeation
835 studies can promote a reversible disruption of the skin layers and long-time used for in vitro
836 skin permeation studies is able to promote higher degree of skin hydration and possible
837 changes of this biological material reducing its barrier function. Therefore, preliminary tape
838 stripping experiments were performed on porcine ear (skin remained on the cartilage during
839 the experiment) to investigate penetration of CBD into the skin after shorter exposure time,
840 utilizing the same infinite dose setting. The samples were obtained after 2 h of application of
841 the two examined formulations and the CBD amount was quantified using LC-MS/MS
842 technique. In order to achieve more accurate results five independent experiments were
843 performed starting with a preliminary study which was necessary for the determination of the
844 number of strips required for the complete removal of CBD localized in the SC. It is important
845 to mention that the first two tapes removed had to be discarded due to the very high amount
846 of CBD detected in these samples. This phenomenon was especially observed on the area
847 where the hybrids were applied which could be attributed to the bioadhesive properties of
848 chitosan which result in the system remaining on the skin surface even after its removal with
849 the cotton swabs [85].

850



851

852 Figure 9. Diagram representing the stratum corneum concentration of CBD in relation to the
853 cumulative thickness of stratum corneum removed profiles following a 2h application of
854 tested samples (mean \pm SE, n=4).

855

856 The total amount of CBD recovered in the SC for NE (3853.20 ± 543.06 ng/cm²) was
857 slightly higher than for NE/HG (2745.41 ± 1022.44 ng/cm²), but no statistically significant
858 difference was found, despite the remarkable differences in viscosity between the tested
859 formulations. However, as the graph demonstrates (figure 9), there is obvious difference
860 regarding the achieved penetration depth of CBD between the tested formulations. In other
861 words, significantly higher amount of SC was removed with 28 tapes after application of the
862 NE/HG (14.644 ± 8.338 µm) compared to the NE (10.493 ± 3.958 µm). It may be assumed that
863 the cohesion of the corneocytes might have been decreased after application of the NE/HG
864 as aforementioned in the previous paragraph due to the chitosan interaction with the SC. It
865 has been mentioned in previous studies that chitosan demonstrates permeation-promoting
866 properties through diverse mechanisms including the alteration of the conformation of
867 keratins reducing the cohesion of the SC, the action on the tight junctions and the increase of
868 water content [81,86]. Additionally, comparing this finding with in vitro permeation results, it
869 appears that skin occlusion potentiated the observed effect, leading to improved CBD delivery
870 during the prolonged test duration. These results indicate a rapid and high permeation

1
2
3
4
5
6
7
8
9
10
11
12
13
14
15
16
17
18
19
20
21
22
23
24
25
26
27
28
29
30
31
32
33
34
35
36
37
38
39
40
41
42
43
44
45
46
47
48
49
50
51
52
53
54
55
56
57
58
59
60
61
62
63
64
65

871 through the SC suggesting that the proposed nanocarriers are suitable for the transdermal
872 delivery of CBD with the hybrid system demonstrated enhanced properties as a delivery
873 system for percutaneous delivery. In order to confirm the relevance of the obtained data,
874 additional experiments utilizing finite dose setting, representative for common in-use
875 conditions, are needed.

876

877 **4. Conclusion**

878 The goal of the present research was to develop a novel delivery system for the
879 effective transdermal administration of lipophilic bioactive compounds that would avoid
880 topical irritation caused by burst release. For that reason, O/W nanoemulsions and the
881 corresponding nanoemulsion-filled chitosan hydrogels were successfully developed as
882 encapsulation media of CBD. The proposed formulation method could be widely used since it
883 is simple and rapid in contrast to other previously reported methods [53]. Initially a series of
884 O/W nanoemulsions were formulated and studied using DLS to evaluate their droplet size,
885 size distribution, and stability in relation to their composition and preparation method.
886 Monodispersed and stable for three months, nanoemulsions containing EVOO in the oil phase
887 were selected as more suitable for the encapsulation of CBD. These nanoemulsions were
888 prepared with low energy input in the absence of co-solvent or any permeation enhancers.
889 Then, CBD-loaded nanoemulsions were added in chitosan hydrogels and the resulting hybrid
890 formulations were structurally characterized by means of EPR, SAXS, confocal microscopy and
891 cryo-EM. A crucial part of the present study was the elucidation of the structure of the
892 formulated systems since it has great impact on the release of the encapsulated bioactive
893 compound [87–89]. Specifically, this is the first study having in the centre of attention the
894 investigation of possible structural changes after the incorporation of the nanoemulsion into
895 the hydrogel that could in turn lead to differences in the release of the encapsulated CBD.
896 Experimental results from EPR spin probing showed that membrane dynamics in terms of local
897 viscosity, order and polarity in nanoemulsion-filled hydrogels were similar to the
898 corresponding nanoemulsions in the absence of CBD. However, the observed changes in
899 rotational correlation time values between the CBD-loaded nanoemulsions and
900 nanoemulsion-filled hydrogels provide an indication that the hybrid systems could release
901 more effectively the encapsulated compound. Confocal micrographs showed the existence of
902 spherical oil droplets of comparable sizes in both formulations. Empty and CBD-loaded
903 nanoemulsions characterized via cryo-EM showed spherical structures and droplet diameters

1
2
3
4
5
6
7
8
9
10
11
12
13
14
15
16
17
18
19
20
21
22
23
24
25
26
27
28
29
30
31
32
33
34
35
36
37
38
39
40
41
42
43
44
45
46
47
48
49
50
51
52
53
54
55
56
57
58
59
60
61
62
63
64
65

904 that agreed well with the DLS results. SAXS results also indicated that the spherical structure
905 and the size of the nanoemulsions were not affected by their incorporation in the hydrogel.

906 Subsequently, cell viability was assessed in the absence and presence of CBD
907 indicating that both the nanoemulsions and the hybrid hydrogels present high
908 biocompatibility and possibly dose-dependent induction of cell proliferation. It is worth noting
909 that the developed nanocarriers were administered at very high concentrations compared to
910 previous similar systems that have been reported in the literature without showing the
911 corresponding cytotoxicity [53,90]. These results are expected due to the low surfactant
912 concentration used for the formulation of the systems since it is widely known that various
913 synthetic surfactants could present dose-dependent toxicity [91]. Furthermore, the addition
914 of extra virgin olive oil as component of the oil phase also enhances the biocompatibility of
915 the systems since its health promoting properties are established [70,92]. Finally, to evaluate
916 the suitability of the nanoemulsions and the hybrid systems as vehicles for the transdermal
917 delivery of CBD *ex vivo* evaluation was performed using porcine ear skin as the model
918 membrane. The bioactive compound was detected in the acceptor medium of Franz diffusion
919 cells first from the hybrid systems, followed by the nanoemulsions and sustained release was
920 observed from both the nanocarriers under study during the 30 h of the experiment.
921 Additionally, differential tape stripping technique demonstrated high permeability of CBD
922 through the *stratum corneum* with the hybrid system exhibiting enhanced penetration
923 possibly due to change of the structure of the *stratum corneum* in the presence of chitosan.
924 Hence, the present study could be a new approach for the development of effective and at
925 the same time non-toxic transdermal delivery vehicles since it suggests that the presence of
926 penetration enhancers, alcohols or high concentrations of co-surfactants or other possibly
927 toxic components is not necessary to obtain effective transdermal delivery of a strongly
928 lipophilic substance such as CBD [93–96].

929 Therefore, these systems could be ideal candidates for use as carriers for
930 (trans)dermal delivery of highly lipophilic bioactive compounds. In the future, their ability to
931 simultaneously encapsulate lipophilic and hydrophilic bioactive substances in order to obtain
932 synergistic action and improved biological effects remains to be studied.

937 **Acknowledgments:** We thank M. Ahmed Bentaleb, Univ. Bordeaux, CRPP, France, for his
938 contribution on the execution of the SAXS experiments.

939 PLK, FLK and FH were supported by the Federal Ministry of Education and Research (BMBF,
940 ZIK program) [grant numbers 03Z22HN23 and 03Z22HI2 (to P.L.K.)]; the European Regional
941 Development Fund for Saxony-Anhalt [grant number EFRE: ZS/2016/04/78115 (to P.L.K.)], and
942 the Martin Luther University Halle-Wittenberg. AX thanks the University of Bordeaux, IdEx
943 Visiting Scholars for his stay.

944 **Funding:** This research received no external funding.

945 **Conflicts of Interest:** The authors declare no conflict of interest.

946

947

948 **References**

- 949 [1] WHO, CANNABIDIOL (CBD) Critical Review Report Expert Committee on Drug
950 Dependence Fortieth Meeting, 2018.
- 951 [2] N.A. Jones, S.E. Glyn, S. Akiyama, T.D. Hill, A.J. Hill, S.E. Weston, M.D. Burnett, Y.
952 Yamasaki, G.J. Stephens, B.J. Whalley, C.M. Williams, Cannabidiol exerts anti-
953 convulsant effects in animal models of temporal lobe and partial seizures, *Seizure*.
954 (2012) 344–352. <https://doi.org/https://doi.org/10.1016/j.seizure.2012.03.001>.
- 955 [3] N. Poulia, F. Delis, C. Brakatselos, G. Ntoulas, M.Z. Asprogerakas, K. Antoniou, CBD
956 Effects on Motor Profile and Neurobiological Indices Related to Glutamatergic
957 Function Induced by Repeated Ketamine Pre-Administration, *Front Pharmacol.* 12
958 (2021). <https://doi.org/https://doi.org/10.3389/fphar.2021.74693>.
- 959 [4] Baswan Sudhir M, Klosner Allison E, Glynn Kelly, Rajgopal Arun, Malik Kausar, Yim
960 Sunghan, Stern Nathan, Therapeutic potential of cannabidiol (CBD) for skin health
961 and disorders, *Clin Cosmet Investig Dermatol.* 13 (2020).
962 <https://doi.org/10.2147/CCID.S286411>.
- 963 [5] S.C. Britch, S. Babalonis, S.L. Walsh, Cannabidiol: pharmacology and therapeutic
964 targets, *Psychopharmacology (Berl).* 238 (2021) 9–28.
965 <https://doi.org/10.1007/S00213-020-05712-8>.
- 966 [6] E. Kozela, A. Juknat, N. Kaushansky, N. Rimmerman, Ben-Nun Avraham, Vogel Zvi,
967 Cannabinoids decrease the th17 inflammatory autoimmune phenotype, *Journal of*
968 *Neuroimmune Pharmacology.* 8 (2013) 1265–1276. [https://doi.org/10.1007/s11481-](https://doi.org/10.1007/s11481-013-9493-1)
969 [013-9493-1](https://doi.org/10.1007/s11481-013-9493-1).
- 970 [7] A. Rahimi, M. Faizi, F. Talebi, F. Noorbakhsh, F. Kahrizi, N. Naderi, Interaction
971 between the protective effects of cannabidiol and palmitoylethanolamide in

1 972 experimental model of multiple sclerosis in C57BL/6 mice, *Neuroscience*. (2015) 279–
2 973 287. <https://doi.org/https://doi.org/10.1016/j.neuroscience.2015.01.030>.

3
4 974 [8] G. Esposito, M. Pesce, L. Seguella, W. Sanseverino, J. Lu, C. Corpetti, G. Sarnelli, The
5 975 potential of cannabidiol in the COVID-19 pandemic, *Br J Pharmacol*. 177 (2020) 4967–
6 976 4970. <https://doi.org/10.1111/BPH.15157>.

7
8 977 [9] B. Malinowska, M. Baranowska-Kuczko, A. Kicman, E. Schlicker, Opportunities,
9 978 challenges and pitfalls of using cannabidiol as an adjuvant drug in COVID-19,
10 979 *Mdpi.Com*. (2021) 22. <https://doi.org/10.3390/ijms22041986>.

11
12
13 980 [10] Watson S., Benson J., Joy JE, Marijuana and medicine: assessing the science base: a
14 981 summary of the 1999 Institute of Medicine report, *Arch Gen Psychiatry*. 6 (2000)
15 982 547–552. <https://doi.org/10-1001/pubs.Arch Gen Psychiatry-ISSN-0003-990x-57-6-ynv9343>.
16 983

17
18
19 984 [11] A. Hazekamp, The Trouble with CBD Oil, *Med Cannabis Cannabinoids*. 1 (2018) 65–72.
20 985 <https://doi.org/10.1159/000489287>.

21
22
23 986 [12] H. Mahmoudinoodezh, S. Telukutla, S. Bhangu, A. Bachari, F. Cavalieri, N. Mantri, The
24 987 Transdermal Delivery of Therapeutic Cannabinoids, *Pharmaceutics*. 14 (2022).
25 988 <https://doi.org/https://doi.org/10.3390/pharmaceutics14020438>.

26
27
28 989 [13] A. Tijani, D. Thakur, D. Mishra, D. Frempong, U.I. Chukwunyere, A. Puri, Delivering
29 990 therapeutic cannabinoids via skin: Current state and future perspectives, *Journal of*
30 991 *Controlled Release*. 334 (2021) 427–451.
31 992 <https://doi.org/https://doi.org/10.1016/j.jconrel.2021.05.005>.

32
33
34 993 [14] Prakash U. R.T., P., Thiagarajan, Nanoemulsions for drug delivery through different
35 994 routes, *Research in Biotechnology*. 2 (2011). [https://agris.fao.org/agris-
36 995 search/search.do?recordID=AE2019100853](https://agris.fao.org/agris-search/search.do?recordID=AE2019100853).

37
38
39 996 [15] M. Lodzki, B. Godin, L. Rakou, R. Mechoulam, R. Gallily, E. Touitou, Cannabidiol—
40 997 transdermal delivery and anti-inflammatory effect in a murine model, *Journal of*
41 998 *Controlled Release*. 93 (2003) 377–387.
42 999 <https://doi.org/https://doi.org/10.1016/j.jconrel.2003.09.001>.

43
44
45 1000 [16] D.C. Hammell, L.P. Zhang, F. Ma, S.M. Abshire, S.L. Mcilwrath, A.L. Stinchcomb, K.N.
46 1001 Westlund, Transdermal cannabidiol reduces inflammation and pain-related
47 1002 behaviours in a rat model of arthritis, *Wiley Online Library*. 20 (2015) 936–948.
48 1003 <https://doi.org/10.1002/ejp.818>.

49
50
51 1004 [17] I. Scheffer, J. Hulihan, J. Messenheimer, S. Ali, N. Keenan, J. Griesser, L.G. Sadleir,
52 1005 Safety and Tolerability of Transdermal Cannabidiol Gel in Children with
53 1006 Developmental and Epileptic Encephalopathies: A Nonrandomized Controlled Trial,
54 1007 *JAMA Netw Open*. 4 (2021).
55 1008 <https://doi.org/doi:10.1001/jamanetworkopen.2021.23930>.

56
57
58
59
60
61
62
63
64
65

- 1009 [18] G. Gonzalez-Cuevas, R. Martin-Fardon, T.M. Kerr, D.G. Stouffer, L.H. Parsons, D.C.
1010 Hammell, S.L. Banks, A.L. Stinchcomb, F. Weiss, Unique treatment potential of
1011 cannabidiol for the prevention of relapse to drug use: preclinical proof of principle,
1012 *Neuropsychopharmacology* 2018 43:10. 43 (2018) 2036–2045.
1013 <https://doi.org/10.1038/s41386-018-0050-8>.
- 1014 [19] I. Theochari, A. Xenakis, V. Papadimitriou, Nanocarriers for effective drug delivery,
1015 *Smart Nanocontainers: Micro and Nano Technologies*. (2020) 315–341.
1016 <https://doi.org/10.1016/B978-0-12-816770-0.00019-8>.
- 1017 [20] J. Patra, G. Das, L. Fraceto, E. Campos, M. Rodriguez-Torres, L. Acosta-Torres, L. Diaz-
1018 Torres, R. Grillo, M. Swamy, S. Sharma, S. Habtemariam, H. Shin, Nano based drug
1019 delivery systems: recent developments and future prospects, *J Nanobiotechnology*.
1020 16 (2018) 1–33. <https://doi.org/https://doi.org/10.1186/s12951-018-0392-8>.
- 1021 [21] P. Vega-Vásquez, N.S. Mosier, J. Irudayaraj, Nanoscale Drug Delivery Systems: From
1022 Medicine to Agriculture, *Front Bioeng Biotechnol*. 8 (2020).
1023 <https://doi.org/10.3389/FBIOE.2020.00079/FULL>.
- 1024 [22] M. Mitchell, M. Billingsley, R. Haley, M. Wechsler, A. Peppas, R. Langer, Engineering
1025 precision nanoparticles for drug delivery, *Nat Rev Drug Discov*. 20 (2021) 101–124.
1026 <https://doi.org/https://doi.org/10.1038/s41573-020-0090-8>.
- 1027 [23] A. Gupta, B.H. Eral, A.T. Hatton, P.S. Doyle, Nanoemulsions: formation, properties
1028 and applications, *Soft Matter*. 12 (2016) 2826–2841.
1029 <https://doi.org/10.1039/C5SM02958A>.
- 1030 [24] T. Mason, J. Wilking, K. Meleson, C. Chang, S. Graves, Nanoemulsions: formation,
1031 structure, and physical properties, *Journal of Physics: Condensed Matter*. 18 (2006).
1032 <https://doi.org/https://doi.org/10.1088/0953-8984/18/41/R01>.
- 1033 [25] A. Naseema, L. Kovooru, A. Behera, K. Kumar, P. Srivastava, A critical review of
1034 synthesis procedures, applications and future potential of nanoemulsions, *Adv*
1035 *Colloid Interface Sci*. 287 (2021).
1036 <https://doi.org/https://doi.org/10.1016/j.cis.2020.102318>.
- 1037 [26] D.J. McClements, Nanoemulsions versus microemulsions: terminology, differences,
1038 and similarities, *Soft Matter*. 8 (2012) 1719–1729.
1039 <https://doi.org/10.1039/C2SM06903B>.
- 1040 [27] N.A. Peppas, P. Bures, W. Leobandung, H. Ichikawa, Hydrogels in pharmaceutical
1041 formulations, *European Journal of Pharmaceutics and Biopharmaceutics*. 50 (2000)
1042 27–46. [https://doi.org/10.1016/S0939-6411\(00\)00090-4](https://doi.org/10.1016/S0939-6411(00)00090-4).
- 1043 [28] E.M. Ahmed, Hydrogel: Preparation, characterization, and applications: A review, *J*
1044 *Adv Res*. 6 (2015) 105–121. <https://doi.org/10.1016/J.JARE.2013.07.006>.

- 1045 [29] R. Batista, C. Otoni, P. Espitia, Fundamentals of chitosan-based hydrogels: elaboration
1046 and characterization techniques, *Materials for Biomedical Engineering*. (2019) 61–81.
1047 <https://doi.org/https://doi.org/10.1016/B978-0-12-816901-8.00003-1>.
- 1048 [30] E. Mitsou, V. Pletsas, G. Sotiroudis, P. Panine, M. Zoumpantioti, A. Xenakis,
1049 Development of a microemulsion for encapsulation and delivery of gallic acid. The
1050 role of chitosan, *Colloids Surf B Biointerfaces*. 190 (2020).
1051 <https://doi.org/https://doi.org/10.1016/j.colsurfb.2020.110974>.
- 1052 [31] T. Hoare, D. DS Kohane, Hydrogels in drug delivery: Progress and challenges, *Polymer*
1053 (Guildf). 49 (2008) 1993–2007.
1054 <https://doi.org/https://doi.org/10.1016/j.polymer.2008.01.027>.
- 1055 [32] E. Dickinson, Emulsion gels: The structuring of soft solids with protein-stabilized oil
1056 droplets, *Food Hydrocoll*. 28 (2012) 224–241.
1057 <https://doi.org/10.1016/J.FOODHYD.2011.12.017>.
- 1058 [33] O. Torres, N. Tena, B. Murray, A. Sarkar, Novel starch based emulsion gels and
1059 emulsion microgel particles: Design, structure and rheology, *Carbohydr Polym*. 178
1060 (2017) 86–94. <https://doi.org/https://doi.org/10.1016/j.carbpol.2017.09.027>.
- 1061 [34] T. Farjami, A. Madadlou, An overview on preparation of emulsion-filled gels and
1062 emulsion particulate gels, *Trends Food Sci Technol*. 86 (2019) 85–94.
1063 <https://doi.org/https://doi.org/10.1016/j.tifs.2019.02.043>.
- 1064 [35] G. Vaz, A. Clementino, E. Mitsou, E. Ferrari, F. Buttini, C. Sissa, A. Xenakis, F. Sonvico,
1065 C. Dora, In Vitro Evaluation of Curcumin- and Quercetin-Loaded Nanoemulsions for
1066 Intranasal Administration: Effect of Surface Charge and Viscosity, *Pharmaceutics*
1067 2022, Vol. 14, Page 194. 14 (2022) 194.
1068 <https://doi.org/10.3390/PHARMACEUTICS14010194>.
- 1069 [36] F. Hamdi, C. Tüting, D.A. Semchonok, K.M. Visscher, F.L. Kyrillis, A. Meister, I. Skolidis,
1070 L. Schmidt, C. Parthier, M.T. Stubbs, P.L. Kastritis, 2.7 Å cryo-EM structure of vitrified
1071 M. Musculus H-chain apoferritin from a compact 200 keV cryo-microscope, *PLoS One*.
1072 15 (2020). <https://doi.org/10.1371/JOURNAL.PONE.0232540>.
- 1073 [37] I. Pantelić, T. Ilić, B. Marković, S. Savić, M. Lukić, S. Savić, A stepwise protocol for drug
1074 permeation assessment that combines heat-separated porcine ear epidermis and
1075 vertical diffusion cells, *Doiserbia.Nb.Rs*. 72 (2018) 47–53.
1076 <https://doi.org/10.2298/HEMIND170726019P>.
- 1077 [38] T. Ilić, S. Savić, B. Batinić, B. Marković, M. Schmidberger, D. Lunter, S. Savić,
1078 Combined use of biocompatible nanoemulsions and solid microneedles to improve
1079 transport of a model NSAID across the skin: In vitro and in vivo studies, *European*
1080 *Journal of Pharmaceutical Sciences*. 125 (2018) 110–119.
1081 <https://doi.org/https://doi.org/10.1016/j.ejps.2018.09.023>.

- 1082 [39] V. Klang, J. Schwarz, B. Lenobel, M. Nadj, J. Auböck, M. Wolzt, C. Valenta, In vitro vs.
 1083 in vivo tape stripping: Validation of the porcine ear model and penetration
 1084 assessment of novel sucrose stearate emulsions, *Uropean Journal of Pharmaceutics*
 1085 and *Biopharmaceutics*. 80 (2012) 604–614.
 1086 <https://doi.org/https://doi.org/10.1016/j.ejpb.2011.11.009>.
- 1087 [40] S. Demisli, E. Mitsou, V. Pletsa, A. Xenakis, V. Papadimitriou, Development and study
 1088 of nanoemulsions and nanoemulsion-based hydrogels for the encapsulation of
 1089 lipophilic compounds, *Nanomaterials*. 10 (2020).
 1090 <https://doi.org/10.3390/nano10122464>.
- 1091 [41] L. Peng, C. Liu, C. Kwan, K. Huang, Optimization of water-in-oil nanoemulsions by
 1092 mixed surfactants, *Colloids Surf A Physicochem Eng Asp*. 370 (2010) 136–142.
 1093 <https://doi.org/https://doi.org/10.1016/j.colsurfa.2010.08.060>.
- 1094 [42] M. Fanun, Properties of microemulsions with mixed nonionic surfactants and citrus
 1095 oil, *Colloids Surf A Physicochem Eng Asp*. 369 (2010) 246–252.
 1096 <https://doi.org/10.1016/J.COLSURFA.2010.08.028>.
- 1097 [43] A. Xenakis, V. Papadimitriou, T. Sotiroudis, Colloidal structures in natural oils, *Curr*
 1098 *Opin Colloid Interface Sci*. 15 (2010) 55–60.
 1099 <https://doi.org/https://doi.org/10.1016/j.cocis.2009.11.007>.
- 1100 [44] J.S. Komaiko, D.J. McClements, Formation of Food-Grade Nanoemulsions Using Low-
 1101 Energy Preparation Methods: A Review of Available Methods, *Compr Rev Food Sci*
 1102 *Food Saf*. 15 (2016) 331–352. <https://doi.org/10.1111/1541-4337.12189>.
- 1103 [45] N.A.N. Azmi, A.A.M. Elgharbawy, S.R. Motlagh, N. Samsudin, H.M. Salleh,
 1104 Nanoemulsions: Factory for Food, Pharmaceutical and Cosmetics, *Processes* 2019,
 1105 Vol. 7, Page 617. 7 (2019) 617. <https://doi.org/10.3390/PR7090617>.
- 1106 [46] M. Gorzynik-Debicka, P. Przychodzen, F. Cappello, A. Kuban-Jankowska, A. Marino
 1107 Gammazza, N. Knap, M. Wozniak, M. Gorska-Ponikowska, Potential health benefits of
 1108 olive oil and plant polyphenols, *Mdpi.Com*. 19 (2018) 547.
 1109 <https://doi.org/10.3390/ijms19030686>.
- 1110 [47] I. Golfomitsou, E. Mitsou, A. Xenakis, V. Papadimitriou, Development of food grade
 1111 O/W nanoemulsions as carriers of vitamin D for the fortification of emulsion based
 1112 food matrices: A structural and activity study, *J Mol Liq*. 268 (2018) 734–742.
 1113 <https://doi.org/https://doi.org/10.1016/j.molliq.2018.07.109>.
- 1114 [48] S. Demisli, I. Theochari, P. Christodoulou, M. Zervou, A. Xenakis, V. Papadimitriou,
 1115 Structure, activity and dynamics of extra virgin olive oil-in-water nanoemulsions
 1116 loaded with vitamin D3 and calcium citrate, *J Mol Liq*. 306 (2020).
 1117 <https://doi.org/https://doi.org/10.1016/j.molliq.2020.112908>.
- 1118 [49] I. Theochari, E. Mitsou, I. Nikolic, T. Ilic, V. Dobricic, V. Pletsa, V. Papadimitriou,
 1119 Colloidal nanodispersions for the topical delivery of Ibuprofen: Structure, dynamics

1120 and bioperformances, *J Mol Liq.* 334 (2021).
1121 <https://doi.org/https://doi.org/10.1016/j.molliq.2021.116021>.

1122 [50] C. Zhao, L. Wei, B. Yin, F. Liu, J. Li, X. Liu, J. Wang, Encapsulation of lycopene within
1123 oil-in-water nanoemulsions using lactoferrin: Impact of carrier oils on
1124 physicochemical stability and bioaccessibility, *Int J Biol Macromol.* 153 (2020) 912–
1125 920. <https://doi.org/https://doi.org/10.1016/j.ijbiomac.2020.03.063>.

1126 [51] L. Palmese, R. Thapa, M. Sullivan, K. Kiick, Hybrid hydrogels for biomedical
1127 applications, *Curr Opin Chem Eng.* 24 (2019) 143–157.
1128 <https://doi.org/https://doi.org/10.1016/j.coche.2019.02.010>.

1129 [52] S. Liu, R. Guo, C. Li, C. Lu, G. Yang, F. Wang, J. Nie, M. Gao, POSS hybrid hydrogels: A
1130 brief review of synthesis, properties and applications, *Eur Polym J.* 143 (2021).
1131 <https://doi.org/https://doi.org/10.1016/j.eurpolymj.2020.110180>.

1132 [53] M. Heidarifard, E. Taghavi, N. Anarjan, Preparation of Nano-Emulsion-Based
1133 Hydrogels Conjugated Curcumin as Model Functional Lipid Bioactive Compound, *J Am
1134 Oil Chem Soc.* 98 (2021) 697–709.
1135 <https://doi.org/https://doi.org/10.1002/aocs.12473>.

1136 [54] E. Hatzara, E. Karatza, S. Avramiotis, A. Xenakis, Spectroscopic mobility probing
1137 studies of lecithin organogels, *Trends in Colloid and Interface Science XVI.* (2004) 94–
1138 97. https://doi.org/10.1007/978-3-540-36462-7_22.

1139 [55] V. Papadimitriou, S. Pispas, S. Syriou, A. Pournara, M. Zoumpanioti, T.G. Sotiroudis, A.
1140 Xenakis, Biocompatible microemulsions based on limonene: formulation, structure,
1141 and applications, *ACS Publications.* 24 (2008) 3380–3386.
1142 <https://doi.org/10.1021/la703682c>.

1143 [56] E. Kalogianni, L. Sklaviadis, S. Nika, I. Theochari, G. Dimitreli, D. Georgiou, V.
1144 Papadimitriou, Effect of oleic acid on the properties of protein adsorbed layers at
1145 water/oil interfaces: An EPR study combined with dynamic interfacial tension
1146 measurements, *Colloids Surf B Biointerfaces.* 158 (2017) 498–506.
1147 <https://doi.org/https://doi.org/10.1016/j.colsurfb.2017.07.022>.

1148 [57] I. Nikolic, E. Mitsou, I. Pantelic, D. Randjelovic, B. Markovic, V. Papadimitriou, S. Savic,
1149 Microstructure and biopharmaceutical performances of curcumin-loaded low-energy
1150 nanoemulsions containing eucalyptol and pinene: Terpenes' role, *European Journal
1151 of Pharmaceutical Sciences.* 142 (2020).
1152 <https://doi.org/https://doi.org/10.1016/j.ejps.2019.105135>.

1153 [58] B. Ozturk, S. Argin, M. Ozilgen, D. McClements, Nanoemulsion delivery systems for
1154 oil-soluble vitamins: Influence of carrier oil type on lipid digestion and vitamin D3
1155 bioaccessibility, *Food Chem.* 187 (2015) 499–506.
1156 <https://doi.org/https://doi.org/10.1016/j.foodchem.2015.04.065>.

- 1
2
3
4
5
6
7
8
9
10
11
12
13
14
15
16
17
18
19
20
21
22
23
24
25
26
27
28
29
30
31
32
33
34
35
36
37
38
39
40
41
42
43
44
45
46
47
48
49
50
51
52
53
54
55
56
57
58
59
60
61
62
63
64
65
- 1157 [59] A. Kwan, G. Davidov-Pardo, Controlled release of flavor oil nanoemulsions
1158 encapsulated in filled soluble hydrogels, *Food Chem.* 250 (2018) 46–53.
1159 <https://doi.org/https://doi.org/10.1016/j.foodchem.2017.12.089>.
- 1160 [60] R. Glaeser, B. Han, R. Csencsits, A. Killilea, A. Pulk, J. Cate, Factors that influence the
1161 formation and stability of thin, cryo-EM specimens, *Biophys J.* 110 (2016) 749–755.
1162 <https://doi.org/https://doi.org/10.1016/j.bpj.2015.07.050>.
- 1163 [61] L. Otrin, A. Witkowska, N. Marušič, Z. Zhao, R. Lira, F. Kyrilis, T. Vidaković-Koch, En
1164 route to dynamic life processes by SNARE-mediated fusion of polymer and hybrid
1165 membranes, *Nat Commun.* 12 (2021) 1–12.
1166 <https://doi.org/https://doi.org/10.1038/s41467-021-25294-z>.
- 1167 [62] N. Marušič, L. Otrin, Z. Zhao, R.B. Lira, F.L. Kyrilis, F. Hamdi, P.L. Kastritis, T. Vidakovic-
1168 Koch, I. Ivanov, K. Sundmacher, R. Dimova, Constructing artificial respiratory chain in
1169 polymer compartments: Insights into the interplay between bo3 oxidase and the
1170 membrane, *Proc Natl Acad Sci U S A.* 117 (2020) 15006–15017.
1171 <https://doi.org/10.1073/PNAS.1919306117>.
- 1172 [63] N. Marusic, L. Otrin, J. Rauchhaus, Z. Zhao, F.L. Kyrilis, F. Hamdi, P.L. Kastritis, R.
1173 Dimova, I. Ivanov, K. Sundmacher, Increased efficiency of charge-mediated fusion in
1174 polymer/lipid hybrid membranes, *Proc Natl Acad Sci U S A.* 119 (2022).
1175 <https://doi.org/10.1073/PNAS.2122468119>.
- 1176 [64] K. Janson, J. Zierath, F. Kyrilis, D. Semchonok, F. Hamdi, I. Skalidis, A. Meister,
1177 Solubilization of artificial mitochondrial membranes by amphiphilic copolymers of
1178 different charge, *Biochimica et Biophysica Acta (BBA)-Biomembranes.* 1863 (2021).
1179 <https://doi.org/https://doi.org/10.1016/j.bbamem.2021.183725>.
- 1180 [65] K. Sejwal, M. Chami, P. Baumgartner, J. Kowal, S.A. Müller, H. Stahlberg,
1181 Proteoliposomes - A system to study membrane proteins under buffer gradients by
1182 cryo-EM, *Nanotechnol Rev.* 6 (2017) 57–74. <https://doi.org/10.1515/NTREV-2016-0081/HTML>.
1183
- 1184 [66] M. Tomšič, M. Bešter-Rogač, A. Jamnik, W. Kunz, D. Touraud, A. Bergmann, O.
1185 Glatter, Nonionic surfactant Brij 35 in water and in various simple alcohols: structural
1186 investigations by small-angle X-ray scattering and dynamic light scattering, *ACS*
1187 *Publications.* 108 (2004) 7021–7032. <https://doi.org/10.1021/jp049941e>.
- 1188 [67] O. Glatter, O. Kratky, H. Kratky, *Small angle x-ray scattering*, Academic Press. (1982).
- 1189 [68] J. de Oca-Avalos, C. Huck-Iriart, V. Borroni, K. Martínez, R. Candal, M. Herrera,
1190 Structural characterization of nanoemulsions stabilized with sodium caseinate and of
1191 the hydrogels prepared from them by acid-induced gelation, *Curr Res Food Sci.* 3
1192 (2020) 113–121. <https://doi.org/https://doi.org/10.1016/j.crfs.2020.03.010>.

1 1193 [69] S. Martín-Peláez, M.I. Covas, M. Fitó, A. Kušar, I. Pravst, Health effects of olive oil
2 1194 polyphenols: Recent advances and possibilities for the use of health claims, *Mol Nutr*
3 1195 *Food Res.* 57 (2013) 760–771. <https://doi.org/10.1002/MNFR.201200421>.

4
5 1196 [70] L. Melguizo-Rodríguez, R. Illescas-Montes, V. Costela-Ruiz, J. Ramos-Torrecillas, E. de
6 1197 Luna-Bertos, O. García-Martínez, C. Ruiz, Antimicrobial properties of olive oil phenolic
7 1198 compounds and their regenerative capacity towards fibroblast cells, *J Tissue Viability*.
8 1199 30 (2021) 372–378. <https://doi.org/https://doi.org/10.1016/j.jtv.2021.03.003>.

10
11 1200 [71] G. Howling, P. Dettmar, P. Goddard, F. Hampson, M. Dornish, E. Wood, The effect of
12 1201 chitin and chitosan on the proliferation of human skin fibroblasts and keratinocytes in
13 1202 vitro, *Biomaterials.* 22 (2001) 2959–2966.
14 1203 [https://doi.org/https://doi.org/10.1016/S0142-9612\(01\)00042-4](https://doi.org/https://doi.org/10.1016/S0142-9612(01)00042-4).

16
17 1204 [72] A. Naseema, P. Padayatti, C. Paulose, Mechanism of wound healing induced by
18 1205 chitosan in streptozotocin diabetic rats, *Curr Sci.* 69 (1995) 461–464.
19 1206 <https://doi.org/https://www.jstor.org/stable/24097159>.

21
22 1207 [73] Z. Zheng, J. Qi, L. Hu, D. Ouyang, H. Wang, Q. Sun, B. Tang, A cannabidiol-containing
23 1208 alginate based hydrogel as novel multifunctional wound dressing for promoting
24 1209 wound healing, *Biomaterials Advances.* 134 (2022).
25 1210 <https://doi.org/https://doi.org/10.1016/j.msec.2021.112560>.

28
29 1211 [74] F. Nigro, C. Cerqueira, A. Rossi, V. Cardoso, A. Vermelho, E. Ricci-Júnior, C. Mansur,
30 1212 Development, characterization and in vitro toxicity evaluation of nanoemulsion-
31 1213 loaded hydrogel based on copaiba oil and coenzyme Q10, *Colloids Surf A*
32 1214 *Physicochem Eng Asp.* 586 (2020).
33 1215 <https://doi.org/https://doi.org/10.1016/j.colsurfa.2019.124132>.

35
36 1216 [75] V. Savić, M. Todosijević, T. Ilić, M. Lukić, E. Mitsou, V. Papadimitriou, S. Savić,
37 1217 Tacrolimus loaded biocompatible lecithin-based microemulsions with improved skin
38 1218 penetration: Structure characterization and in vitro/in vivo performances, *Int J*
39 1219 *Pharm.* 529 (2017) 491–505.
40 1220 <https://doi.org/https://doi.org/10.1016/j.ijpharm.2017.07.036>.

43
44 1221 [76] V. Shah, A. Yacobi, F. Rădulescu, D. Miron, M. Lane, A science based approach to
45 1222 topical drug classification system (TCS), *Int J Pharm.* 491 (2015) 21–25.
46 1223 <https://doi.org/https://doi.org/10.1016/j.ijpharm.2015.06.011>.

48
49 1224 [77] J. Ma, Y. Wang, R. Lu, Mechanism and Application of Chitosan and Its Derivatives in
50 1225 Promoting Permeation in Transdermal Drug Delivery Systems: A Review,
51 1226 *Pharmaceuticals.* 15 (2022). <https://doi.org/https://doi.org/10.3390/ph15040459>.

53
54 1227 [78] J. Berger, M. Reist, J. Mayer, O. Felt, N. Peppas, R. Gurny, Structure and interactions
55 1228 in covalently and ionically crosslinked chitosan hydrogels for biomedical applications,
56 1229 *European Journal of Pharmaceutics and Biopharmaceutics.* 57 (2004) 19–34.
57 1230 [https://doi.org/https://doi.org/10.1016/S0939-6411\(03\)00161-9](https://doi.org/https://doi.org/10.1016/S0939-6411(03)00161-9).

- 1 1231 [79] M. Kaiser, S. Pereira, L. Pohl, S. Ketelhut, B. Kemper, C. Gorzelanny, F. Goycoolea,
2 1232 Chitosan encapsulation modulates the effect of capsaicin on the tight junctions of
3 1233 MDCK cells, *Sci Rep.* 5 (2015) 1–14.
4 1234 <https://doi.org/https://doi.org/10.1038/srep10048>.
5
6 1235 [80] GME., Maghraby, Occlusive versus nonocclusive application in transdermal drug
7 1236 delivery, Springer. 10.1007/978-3-662-53270-6_2.
8
9 1237 [81] W. He, X. Guo, L. Xiao, M. Feng, Study on the mechanisms of chitosan and its
10 1238 derivatives used as transdermal penetration enhancers, *Int J Pharm.* 382 (2009) 234–
11 1239 243. <https://doi.org/https://doi.org/10.1016/j.ijpharm.2009.07.038>.
12
13 1240 [82] G.L. Flynn, R.L. Bronaugh, H.I. Maibach, In vitro percutaneous absorption: principles,
14 1241 fundamentals and applications. , Marcel Dekker Inc. New York. (1985) 17–52.
15
16 1242 [83] D. Bucks, H. Maibach, Occlusion Does Not Uniformly Enhance Penetration In Vivo,
17 1243 CRC Press, 2002. <https://doi.org/10.3109/9780203904015-5>.
18
19 1244 [84] E. Abd, S. Yousef, M. Pastore, K. Telaprolu, Y. Mohammed, S. Namjoshi, M. Roberts,
20 1245 Skin models for the testing of transdermal drugs, *Clin Pharmacol.* 8 (2016) 163–176.
21 1246 <https://doi.org/10.2147/CPAA.S64788>.
22
23 1247 [85] J. Hurler, N. Škalko-Basnet, Potentials of chitosan-based delivery systems in wound
24 1248 therapy: Bioadhesion study, *J Funct Biomater.* 3 (2012) 37–48.
25 1249 <https://doi.org/10.3390/jfb3010037>.
26
27 1250 [86] J. Turner, M. Buschmann, I. Romero-Calvo, A. Sailer, L. Shen, The role of molecular
28 1251 remodeling in differential regulation of tight junction permeability, *Semin Cell Dev*
29 1252 *Biol.* 36 (2014) 204–212.
30 1253 <https://doi.org/https://doi.org/10.1016/j.semcdb.2014.09.022>.
31
32 1254 [87] M. Foldvari, Non-invasive administration of drugs through the skin: challenges in
33 1255 delivery system design, *Pharm Sci Technol Today.* 3 (2000) 417–425.
34 1256 [https://doi.org/https://doi.org/10.1016/S1461-5347\(00\)00317-5](https://doi.org/https://doi.org/10.1016/S1461-5347(00)00317-5).
35
36 1257 [88] M. Elsayed, O. Abdallah, V. Naggar, N. Khalafallah, Lipid vesicles for skin delivery of
37 1258 drugs: reviewing three decades of research, *Int J Pharm.* 332 (2007) 1–16.
38 1259 <https://doi.org/https://doi.org/10.1016/j.ijpharm.2006.12.005>.
39
40 1260 [89] A. Cardoso, E. de Oliveira, K. Coradini, F. Bruinsmann, T. Aguirre, R. Lorenzoni, R.
41 1261 Beck, Chitosan hydrogels containing nanoencapsulated phenytoin for cutaneous use:
42 1262 Skin permeation/penetration and efficacy in wound healing, *Materials Science and*
43 1263 *Engineering: C.* 96 (2019) 205–217.
44 1264 <https://doi.org/https://doi.org/10.1016/j.msec.2018.11.013>.
45
46 1265 [90] L.C. Espinoza, M. Silva-Abreu, B. Clares, M. José Rodríguez-Lagunas, L. Halbaut, M.-A.
47 1266 Cañas, A.C. Calpena, Formulation strategies to improve nose-to-brain delivery of
48 1267 donepezil, *Mdpi.Com.* (2019). <https://doi.org/10.3390/pharmaceutics11020064>.

- 1268 [91] D. Liput, D. Hammell, A. Stinchcomb, K. Nixon, Transdermal delivery of cannabidiol
1269 attenuates binge alcohol-induced neurodegeneration in a rodent model of an alcohol
1270 use disorder, *Pharmacol Biochem Behav.* 111 (2013).
1271 <https://doi.org/https://doi.org/10.1016/j.pbb.2013.08.013>.
- 1272 [92] J. López-Miranda, F. Pérez-Jiménez, E. Ros, R. de Caterina, L. Badimón, M. Covas, N.
1273 Yiannakouris, Olive oil and health: summary of the II international conference on
1274 olive oil and health consensus report, Jaén and Córdoba (Spain) 2008, *Nutrition,*
1275 *Metabolism and Cardiovascular Diseases.* 20 (2008) 284–294.
1276 <https://doi.org/https://doi.org/10.1016/j.numecd.2009.12.007>.
- 1277 [93] K.S. Paudel, D.C. Hammell, R.U. Agu, S. Valiveti, A.L. Stinchcomb, Cannabidiol
1278 bioavailability after nasal and transdermal application: effect of permeation
1279 enhancers, *Taylor & Francis.* 36 (2010) 1088–1097.
1280 <https://doi.org/10.3109/03639041003657295>.
- 1281 [94] B. Thomas, B. Finnin, The transdermal revolution, *Drug Discov Today.* 9 (2004) 697–
1282 703. [https://doi.org/https://doi.org/10.1016/S1359-6446\(04\)03180-0](https://doi.org/https://doi.org/10.1016/S1359-6446(04)03180-0).
- 1283 [95] A.L. Stinchcomb, S. Valiveti, D.C. Hammell, D.R. Ramsey, Human skin permeation of
1284 Δ^8 -tetrahydrocannabinol, cannabidiol and cannabinol, *Journal of Pharmacy and*
1285 *Pharmacology.* 56 (2010) 291–297. <https://doi.org/10.1211/0022357022791>.
- 1286 [96] G. Vanti, L. Grifoni, M. Bergonzi, E. Antiga, F. Montefusco, M. Caproni, A. Bilia,
1287 Development and optimisation of biopharmaceutical properties of a new
1288 microemulgel of cannabidiol for locally-acting dermatological delivery, *Int J Pharm.*
1289 607 (2021). <https://doi.org/https://doi.org/10.1016/j.ijpharm.2021.121036>.
- 1290